ELSEVIER

Nuclear Physics B 580 (2000) 29–57

NUCLEAR PHYSICS B

www.elsevier.nl/locate/npe

# Reconciling the two-loop diagrammatic and effective field theory computations of the mass of the lightest $\mathcal{CP}$-even Higgs boson in the MSSM

M. Carena [a,b], H.E. Haber [c], S. Heinemeyer [d], W. Hollik [e], C.E.M. Wagner [b,f,g], G. Weiglein [b,*]

[a] *FERMILAB, Batavia, IL 60510-0500, USA*
[b] *CERN, TH Division, CH-1211 Geneva 23, Switzerland*
[c] *Santa Cruz Inst. for Part. Phys., Univ. of California, Santa Cruz, CA 95064, USA*
[d] *DESY Theorie, Notkestrasse 85, 22603 Hamburg, Germany*
[e] *Institut für Theoretische Physik, Univ. of Karlsruhe, 76128 Karlsruhe, Germany*
[f] *High Energy Physics Division, Argonne National Lab., Argonne, IL 60439, USA*
[g] *Enrico Fermi Institute, Univ. of Chicago, 5640 Ellis, Chicago, IL 60637, USA*

Received 24 January 2000; accepted 24 March 2000

**Abstract**

The mass of the lightest $\mathcal{CP}$-even Higgs boson of the minimal supersymmetric extension of the standard model (MSSM) has previously been computed including $\mathcal{O}(\alpha\alpha_s)$ two-loop contributions by an on-shell diagrammatic method, while approximate analytic results have also been obtained via renormalization-group-improved effective potential and effective field theory techniques. Initial comparisons of the corresponding two-loop results revealed an apparent discrepancy between terms that depend logarithmically on the supersymmetry-breaking scale, and different dependences of the nonlogarithmic terms on the squark mixing parameter, $X_t$. In this paper, we determine the origin of these differences as a consequence of different renormalization schemes in which both calculations are performed. By reexpressing the on-shell result in terms of $\overline{\rm MS}$ parameters, the logarithmic two-loop contributions obtained by the different approaches are shown to coincide. The remaining difference, arising from genuine nonlogarithmic two-loop contributions, is identified, and its effect on the maximal value of the lightest $\mathcal{CP}$-even Higgs boson mass is discussed. Finally, we show that in a simple analytic approximation to the Higgs mass, the leading two-loop radiative corrections can be absorbed to a large extent into an effective one-loop expression by evaluating the running top quark mass at appropriately chosen energy scales. 

* Corresponding author: Georg.Weiglein@cern.ch

0550-3213/00/$ – see front matter 
PII: S0550-3213(00)00212-1

## 1. Introduction

In the minimal supersymmetric extension of the standard model (MSSM), the mass of the lightest $\mathcal{CP}$-even Higgs boson, $m_h$, is calculable as a function of the MSSM parameters. At tree-level, $m_h$ is a function of the $\mathcal{CP}$-odd Higgs boson mass, $m_A$, and the ratio of vacuum expectation values, $\tan\beta$. Moreover, the tree-level value of $m_h$ is bounded by $m_h \leqslant m_Z|\cos 2\beta|$, which is on the verge of being ruled out by the LEP Higgs search [1,2]. When radiative corrections are taken into account, $m_h$ depends in addition on the MSSM parameters that enter via virtual loops. The radiatively corrected value of $m_h$ depends most sensitively on the parameters of the top-squark (stop) sector: the average squared-mass of the two stops, $M_S^2$, and the off-diagonal stop squared-mass parameter, $m_t X_t$. The stop mixing parameter is $X_t \equiv A_t - \mu\cot\beta$, where $A_t$ is the coefficient of the soft-supersymmetry-breaking stop-Higgs boson trilinear interaction term and $\mu$ is the supersymmetric Higgs mass parameter. The radiatively-corrected value of $m_h^2$ is enhanced by a factor of $G_F m_t^4$ and grows logarithmically as $M_S$ increases [3–6]. In particular, the upper bound for $m_h$ (which is achieved when $m_A \gg m_Z$ and $\tan\beta \gg 1$) is significantly increased beyond its tree-level upper bound of $m_Z$.

The complete one-loop diagrammatic computation of $m_h$ has been carried out in Refs. [7–9]. However, for $M_S \gg m_t$, the logarithmically enhanced terms are significant (in particular, the most significant logarithmic terms are those that are enhanced by the $G_F m_t^4$ pre-factor noted above), in which case leading-logarithmic corrections from higher-loop contributions must be included. These terms can be summed via renormalization group techniques. The result of these corrections is to reduce the one-loop upper bound on $m_h$. For $M_S \lesssim \mathcal{O}(1\ \text{TeV})$, it is found that $m_h \lesssim 125$ GeV, where the maximum is reached at large $m_A$ and $\tan\beta$ when $M_S$ is maximal and $X_t \simeq \pm\sqrt{6}\,M_S$ (the so-called "maximal-mixing" value for stop mixing). However, subleading two-loop corrections may not be negligible, and a more complete two-loop computation is required.

The full diagrammatic calculations lead to very complicated expressions for the radiatively corrected value of $m_h$. Effective potential and effective field theory techniques have been developed which can extract the dominant contributions to the Higgs mass radiative corrections (when $M_S$ is large), resulting in a simpler analytic expression for $m_h$. These methods also provide a natural setting for renormalization group improvement. Although the exact solution of the renormalization group equations (RGEs) must be obtained numerically, the iterative solution of the RGEs can easily yield simple analytic expressions for the one-loop and two-loop leading logarithmic contributions to $m_h$. These leading logarithms can also be obtained by expanding the complete diagrammatic results in the limit of $M_S \gg m_t$, and this serves as an important check of the various computations.

The effective potential method (for a review, see [10]) provides an important tool for evaluating the Higgs mass beyond the tree-level. It can be used to provide a short-cut for the calculation of certain combinations of Higgs boson two-point functions that arise in the diagrammatic computation. The effective field theory (EFT) approach [11] provides a powerful method for isolating the leading terms of the Higgs mass radiative corrections when $M_S \gg m_t$. In this formalism, one matches the full supersymmetric theory above

$M_S$ to an effective standard model with supersymmetric particles decoupled below $M_S$. The standard model couplings in the $\overline{\rm MS}$ scheme are fixed at $M_S$ by supersymmetric matching conditions. Standard model RGEs are then used to evolve these couplings down to the electroweak scale (either $m_t$ or $m_Z$). While the stops are decoupled at $M_S$, the stop mixing (so-called "threshold") effects are incorporated by modifying the matching conditions at $M_S$. With the use of effective potential techniques, the EFT formalism and the iteration of the RGEs to two-loops, the leading contributions to the radiatively-corrected Higgs mass was obtained in analytic form in Refs. [12–15]. These results included the full one-loop leading logarithmic corrections and one-loop leading squark-mixing threshold corrections, the two-loop leading double-logarithmic corrections and the two-loop leading logarithmic squark-mixing threshold corrections up to $\mathcal{O}(h_t^2\alpha_s)$ and $\mathcal{O}(h_t^4)$, where $h_t$ is the Higgs–top quark Yukawa coupling.

In order to extend the above results, genuine two-loop computations are required. The first two-loop diagrammatic computation was performed in Ref. [16] in the limit of $m_A \gg m_Z$ and $\tan\beta \gg 1$ (where $m_h$ attains its maximal bound), where only terms of $\mathcal{O}(h_t^4)$ and $\mathcal{O}(h_t^2\alpha_s)$ were evaluated, and all squark mixing effects were neglected. More recently, a more complete two-loop diagrammatic computation of the dominant contributions at $\mathcal{O}(\alpha\alpha_s)$ to the neutral $\mathcal{CP}$-even Higgs boson masses has been performed [17–19]. This result was obtained for arbitrary values of $m_A$, $\tan\beta$ and the stop-mixing parameter $X_t$. This two-loop result, which had been obtained first in the on-shell scheme, was subsequently combined [18,19] with the complete diagrammatic one-loop on-shell result of Ref. [8] and the leading two-loop Yukawa corrections of $\mathcal{O}(h_t^4)$ obtained by the EFT approach [12–15]. The resulting two-loop expression was then expressed in terms of the top-quark mass in the $\overline{\rm MS}$ scheme. By comparing the final expression with the results obtained in Refs. [12–15], it was shown that the upper bound on the lightest Higgs mass was shifted upwards by up to 5 GeV, an effect that is more pronounced in the low $\tan\beta$ region.

Besides the shift in the upper bound of $m_h$, apparent deviations between the explicit diagrammatic two-loop calculation and the results of the EFT computation were observed in the dependence of $m_h$ on the stop-mixing parameter $X_t$. While the value of $X_t$ that maximizes the lightest $\mathcal{CP}$-even Higgs mass is $(X_t)_{\rm max} \simeq \pm\sqrt{6}\,M_S \approx \pm 2.4\,M_S$ in the results of Refs. [12–15], the corresponding on-shell two-loop diagrammatic computation found a maximal value for $m_h$ at $(X_t)_{\rm max} \approx 2M_S$.[1] Moreover, in the results of Refs. [12–15], $m_h$ is symmetric under $X_t \to -X_t$ and has a (local) minimum at $X_t = 0$. In contrast, the two-loop diagrammatic computation yields $m_h$ values for positive and negative $X_t$ that differ significantly from each other and the local minimum in $m_h$ is shifted slightly away from $X_t = 0$ [20]. A similar conclusion was reached in Ref. [21], which used an effective potential calculation to extend the results of Ref. [16] to the case of non-zero stop mixing.

[1] A local maximum for $m_h$ is also found for $X_t \simeq -2M_S$, although the corresponding value of $m_h$ at $X_t \simeq +2M_S$ is significantly larger [19,20].

A closer comparison of results of the EFT computation of the radiatively-corrected Higgs mass and the two-loop diagrammatic computation at first sight revealed a surprising discrepancy. Namely, the two-loop leading logarithmic squark-mixing threshold corrections at $\mathcal{O}(h_t^2\alpha_s)$ of the former do not appear to match the results of the latter. In this paper, we shall show that this apparent discrepancy in the leading-logarithmic contributions is caused by the different renormalization schemes employed in the two approaches. While the original two-loop diagrammatic computations of Ref. [17] were performed in an on-shell scheme, the results of the EFT approach are most naturally carried out in the $\overline{\rm MS}$ scheme. In comparing results obtained within different renormalization schemes in terms of the (not directly observable) parameters $X_t$ and $M_S$, one has to take into account the fact that these parameters are renormalization-scheme dependent. The effect of this scheme dependence first enters into the calculation of $m_h$ at the two-loop level. In order to allow a detailed comparison between the results of the different approaches we derive relations between these parameters in the two different schemes. We apply these relations to reexpress the diagrammatic on-shell result in terms of $\overline{\rm MS}$ parameters. In this way we show that the leading logarithmic two-loop contributions in the two approaches in fact coincide. The remaining numerical difference between the diagrammatic calculation in the $\overline{\rm MS}$ scheme and the result obtained by the EFT approach can thus be identified with new threshold effects due to nonlogarithmic two-loop terms contained in the diagrammatic result. We furthermore show that in the analytic approximation employed in this paper, the dominant numerical contribution of these terms can be absorbed into an effective one-loop expression by choosing an appropriate scale for the running top-quark mass in different terms of the expression.

This paper is organized as follows. To simplify the analysis, we focus completely on the radiatively corrected Higgs squared-mass in the "leading $m_t^4$ approximation" (in which only the dominant loop corrections proportional to $m_t^2 h_t^2 \sim G_F m_t^4$ are kept). In addition, we choose a very simple form for the stop squared-mass matrix, which significantly simplifies the subsequent analysis while maintaining the most important features of the general result. In Section 2 we sketch the derivation of the EFT result for the radiatively-corrected Higgs mass of Refs. [12–15] at $\mathcal{O}(m_t^2 h_t^2 \alpha_s)$ in the limit of $m_A \gg m_Z$. The corresponding result of the two-loop diagrammatic computation, under the same set of approximations, is outlined in Section 3. In order to compare the two results, we must convert on-shell quantities to $\overline{\rm MS}$ quantities. In Section 4 we derive the relations between the on-shell and the $\overline{\rm MS}$ values of the parameters $m_t$, $X_t$ and $M_S$ in the limit of large $M_S$. Details of the exact calculation are given in Appendix A, while explicit relations between the on-shell and the $\overline{\rm MS}$ parameters up to $\mathcal{O}(m_t^4/M_S^4)$ are given in Appendix B. In Section 5 the diagrammatic on-shell result is expressed in terms of $\overline{\rm MS}$ parameters and compared to the result of the EFT computation of Section 2. The logarithmic contributions are shown to coincide, and the remaining difference caused by nonlogarithmic two-loop terms is analyzed. We argue that the remaining difference can be minimized by improving the EFT computation by taking into account the stop-mixing threshold contribution to the running top-quark mass. In addition, we demonstrate that in a simple analytic approximation to the Higgs mass, one can absorb the dominant two-loop contributions into an effective one-

loop expression. In Section 6, we summarize our results and discuss suggestions for future improvements.

## 2. Effective field theory approach

At the tree level, the mass matrix of the neutral $\mathcal{CP}$-even Higgs bosons in the basis of weak eigenstates of definite hypercharge $-1$ and $+1$ respectively can be expressed in terms of $m_Z$, $m_A$ and $\tan\beta \equiv v_2/v_1$ as follows:

$$\mathcal{M}_H^{2,\text{tree}} = \begin{pmatrix} m_A^2 \sin^2\beta + m_Z^2 \cos^2\beta & -(m_A^2 + m_Z^2)\sin\beta\cos\beta \\ -(m_A^2 + m_Z^2)\sin\beta\cos\beta & m_A^2\cos^2\beta + m_Z^2\sin^2\beta \end{pmatrix}. \tag{1}$$

Diagonalizing this mass matrix yields the tree-level prediction for the lightest neutral $\mathcal{CP}$-even Higgs-boson mass:

$$m_h^{2,\text{tree}} = \tfrac{1}{2}\Big[m_A^2 + m_Z^2 - \sqrt{(m_A^2 + m_Z^2)^2 - 4m_Z^2 m_A^2\cos^2 2\beta}\,\Big]. \tag{2}$$

For simplicity, we shall consider the limit of $m_A \gg m_Z$ and large supersymmetry-breaking masses characterized by a scale $M_S$. Then, at energy scales below $M_S$, the effective low-energy theory consists of the standard model with one Higgs doublet. The corresponding Higgs squared-mass at tree-level is given by $m_h^{2,\text{tree}} = m_Z^2\cos^2 2\beta$. The dominant contributions to the radiatively-corrected Higgs mass within the EFT approach is based on the evaluation of the effective quartic Higgs self-coupling, $\lambda$, evaluated at the scale $Q = \overline{m}_t$. The value of $\lambda(M_S)$ is fixed by the supersymmetric boundary condition, although this value is slightly modified by one-loop threshold effects (denoted below by $\Delta_{\text{th}}\lambda$), due to the decoupling of squarks at $M_S$ with nonzero mixing. One then employs the standard model RGEs to obtain $\lambda(Q)$. Finally, the Higgs mass is obtained via $m_h^2 = 2\lambda(\overline{m}_t)v^2(\overline{m}_t)$ (where $v = 174$ GeV is the Higgs vacuum expectation value). The mass $\overline{m}_t$ denotes the running top-quark mass in the $\overline{\text{MS}}$ scheme at the scale $m_t$. It is related to the on-shell (or pole) top-quark mass $M_t \equiv m_t^{\text{OS}}$ by the following relation:

$$\overline{m}_t \equiv m_{t,\text{SM}}^{\overline{\text{MS}}}(m_t) = \frac{M_t}{1 + \frac{4}{3\pi}\alpha_s(M_t)}, \tag{3}$$

where we have only included the QCD corrections to leading order in $\alpha_s$. In Eq. (3), the subscript 'SM' indicates that the running mass is defined in the usual way, i.e., in terms of the pure Standard Model (gluonic) contributions in the (modified) minimally subtracted dimensional regularization (DREG) scheme [22–24].

The most important contributions to the mass of the lightest $\mathcal{CP}$-even Higgs boson arise from the $t$–$\tilde{t}$ sector of the MSSM, which is characterized by the following squared-mass matrix

$$\mathcal{M}_{\tilde{t}}^2 = \begin{pmatrix} M_{\tilde{t}_L}^2 + m_t^2 + \cos 2\beta\big(\frac{1}{2} - \frac{2}{3}s_W^2\big)m_Z^2 & m_t X_t \\ m_t X_t & M_{\tilde{t}_R}^2 + m_t^2 + \frac{2}{3}\cos 2\beta s_W^2 m_Z^2 \end{pmatrix}, \tag{4}$$

where $X_t \equiv A_t - \mu\cot\beta$. The $\tilde{t}$-masses $m_{\tilde{t}_1}$, $m_{\tilde{t}_2}$ and the mixing angle $\theta_{\tilde{t}}$ are determined at tree-level by diagonalizing $\mathcal{M}_{\tilde{t}}^2$. Neglecting the numerically small contributions proportional to $m_Z^2$ in the stop squared-mass matrix and setting

$$M_{\tilde{t}_L} = M_{\tilde{t}_R} \equiv M_{\rm SUSY}, \qquad M_S^2 \equiv M_{\rm SUSY}^2 + m_t^2 \tag{5}$$

leads to the simplified mass matrix

$$\mathcal{M}_{\tilde{t}}^2 = \begin{pmatrix} M_S^2 & m_t X_t \\ m_t X_t & M_S^2 \end{pmatrix}. \tag{6}$$

In this approximation, the $\tilde{t}$-masses and the mixing angle are given by

$$m_{\tilde{t}_1}^2 = M_S^2 - |m_t X_t|, \qquad m_{\tilde{t}_2}^2 = M_S^2 + |m_t X_t|, \tag{7}$$

$$\theta_{\tilde{t}} = \begin{cases} \frac{\pi}{4} & \text{for } X_t < 0, \\ -\frac{\pi}{4} & \text{for } X_t > 0, \end{cases} \tag{8}$$

where by definition, $m_{\tilde{t}_1} \leqslant m_{\tilde{t}_2}$.

The one-loop threshold corrections to the quartic Higgs self-coupling, induced by the decoupling of stops, lead to a change of the effective quartic Higgs self-coupling at the scale $M_S$,

$$\lambda(M_S) = \tfrac{1}{4}\big(g^2 + g'^2\big)\cos^2 2\beta + \Delta_{\rm th}\lambda, \tag{9}$$

where the first term is the tree-level value of the quartic Higgs self-coupling in the effective low-energy standard model and the second term is the effect of the one-loop threshold corrections at the scale $M_S$ [11,14]:

$$\Delta_{\rm th}\lambda = \frac{3}{8\pi^2} h_t^2 \left\{ \left[ h_t^2 - \frac{1}{8}\big(g^2 + g'^2\big) \right] \left( \frac{X_t^2}{M_S^2} \right) - \frac{1}{12} h_t^2 \left( \frac{X_t^4}{M_S^4} \right) \right\} + \cdots, \tag{10}$$

where all couplings in Eq. (10) should be evaluated at the scale $M_S$. The running Higgs–top quark Yukawa coupling is related to the $\overline{\rm MS}$ running top quark mass:

$$\overline{m}_t(\mu) = h_t(\mu) v(\mu), \tag{11}$$

where the running Higgs vacuum expectation value, $v^2(M_S) = v^2(\overline{m}_t)\,\xi^{-2}(\overline{m}_t)$, is governed by the Higgs field anomalous dimension

$$\xi(\overline{m}_t) = 1 + \frac{3}{32\pi^2} h_t^2(\overline{m}_t) \ln\left( \frac{M_S^2}{\overline{m}_t^2} \right). \tag{12}$$

In obtaining Eq. (10), an expansion in the variable

$$\Delta_{\tilde{t}} \equiv \frac{|m_t X_t|}{M_S^2} = \frac{m_{\tilde{t}_2}^2 - m_{\tilde{t}_1}^2}{m_{\tilde{t}_2}^2 + m_{\tilde{t}_1}^2}, \quad 0 \leqslant \Delta_{\tilde{t}} < 1, \tag{13}$$

has been performed. Terms not explicitly exhibited in Eq. (10) denote the contributions from higher powers in $m_t/M_S$ and $X_t^2/M_S^2$, which arise from the contributions of the $t$–$\tilde{t}$ sector. Contributions from other supersymmetric-breaking sectors have been omitted for simplicity of the presentation. These contributions typically contribute no more than a few GeV to the radiatively-corrected Higgs mass.

As it was shown in Refs. [14,15], one can obtain the two-loop leading-logarithmic correction by expanding the parameter $\lambda$ up to order $[\ln(M_S^2/\overline{m}_t^2)]^2$,

$$\lambda(\overline{m}_t) = \lambda(M_S) - \beta_\lambda(M_S)t + \tfrac{1}{2}\beta'_\lambda(\overline{m}_t)t^2 + \cdots$$
$$= \lambda(M_S) - \beta_\lambda(\overline{m}_t)t - \tfrac{1}{2}\beta'_\lambda(\overline{m}_t)t^2 + \cdots, \tag{14}$$

where $\lambda(M_S)$ is given by Eq. (9) and

$$t \equiv \ln\frac{M_S^2}{\overline{m}_t^2}. \tag{15}$$

Following Ref. [14], we define $\beta_\lambda = a_\lambda\lambda + b_\lambda$. Therefore

$$\lambda(\overline{m}_t) = \lambda(M_S)\big[1 - a_\lambda(\overline{m}_t)t\big] - b_\lambda(\overline{m}_t)t\big[1 - a_\lambda(\overline{m}_t)t\big] - \tfrac{1}{2}\beta'_\lambda(\overline{m}_t)t^2. \tag{16}$$

Here, $1 - a_\lambda(\overline{m}_t)t = \xi^{-4}(\overline{m}_t)$, where $\xi$ is the Higgs field anomalous dimension (Eq. (12)). Multiplying Eq. (16) by $2v^2(\overline{m}_t)$, we obtain an equation for the Higgs squared-mass in the low-energy theory, which takes the following form:

$$m_h^2(\overline{m}_t) = m_h^2(M_S)\,\xi^{-2}(\overline{m}_t) + \Delta_{\rm rad}\,m_h^2(\overline{m}_t), \tag{17}$$

which defines the quantity $\Delta_{\rm rad}m_h^2(\overline{m}_t)$. In Eq. (17),

$$m_h^2(M_S) = 2\lambda(M_S)v^2(M_S), \tag{18}$$

where $\lambda(M_S)$ is given in Eq. (9) with all couplings and masses evaluated at the scale $M_S$.

In the present analysis, we are working in the approximation of $h_b = g = g' = 0$. That is, we focus only on the Higgs–top quark Yukawa and QCD coupling effects. The relevant $\beta$-functions for $\lambda$, $g_3^2$ and $h_t^2$ at scales below the scale $M_S$ are given by (for a useful compilation of two-loop RGEs for the standard model and the MSSM, see [25])

$$16\pi^2\beta_\lambda \equiv 6\big(\lambda^2 + \lambda h_t^2 - h_t^4\big) + \frac{h_t^4}{8\pi^2}\big(15h_t^2 - 16g_3^2\big), \tag{19}$$

$$16\pi^2\beta_{h_t^2} \equiv h_t^2\big(\tfrac{9}{2}h_t^2 - 8g_3^2\big), \tag{20}$$

$$16\pi^2\beta_{g_3^2} \equiv \big(-11 + \tfrac{2}{3}N_f\big)g_3^4, \tag{21}$$

where $\beta_X \equiv dX/d\ln Q^2$ and $N_f$ is the number of quark flavors with masses less than $Q$ (e.g., $N_f = 6$ for scales between $m_t$ and $M_S$). Observe that we have included the dominant strong gauge coupling two-loop contribution to the $\beta$ function of the quartic Higgs self-coupling, since it will contribute once we include all two-loop leading-logarithmic corrections.

Using the above expressions, it is simple to find an approximate formula for the lightest $\mathcal{CP}$-even Higgs mass in the large $m_A$ limit. First, one obtains:

$$\Delta_{\rm rad}m_h^2(\overline{m}_t) = \frac{3}{4\pi^2}\frac{\overline{m}_t^4}{v^2(\overline{m}_t)}t\left[1 + \frac{1}{16\pi^2}\left(\frac{3}{2}h_t^2 - 32\pi\alpha_s\right)t\right], \tag{22}$$

where all couplings in Eq. (22) are evaluated at the scale $Q^2 = \overline{m}_t^2$. To complete the computation of $m_h^2(\overline{m}_t)$ (Eq. (17)), one must evaluate $m_h^2(M_S)$ (see Eq. (18)) in terms of low-energy parameters. This is accomplished by using one-loop renormalization group

evolution to relate $\lambda(M_S)v^2(M_S)$ to $\lambda(\overline{m}_t)v^2(m_t)$. In this way, one finally arrives at the expression: [2]

$$m_h^2 = m_h^{2,\text{tree}} + \frac{3}{4\pi^2}\frac{\overline{m}_t^4}{v^2}\left\{t + \frac{X_t^2}{M_S^2}\left(1 - \frac{X_t^2}{12M_S^2}\right) + \frac{1}{16\pi^2}\left(\frac{3}{2}\frac{\overline{m}_t^2}{v^2} - 32\pi\alpha_s\right)\left[\frac{2X_t^2}{M_S^2}\left(1 - \frac{X_t^2}{12M_S^2}\right)t + t^2\right] + \left(\frac{4\alpha_s}{3\pi} - \frac{5h_t^2}{16\pi^2}\right)t\right\}. \tag{23}$$

The last two terms in Eq. (23) reflect the two-loop single logarithmic dependence induced by the two-loop $\beta$-function contribution to the running of the quartic Higgs self-coupling. It is interesting to note that these two terms are numerically close in size, and they tend to cancel each other in the computation of the Higgs mass. Eq. (23) differs from the one presented in Ref. [13] only in the inclusion of these terms, which although subdominant compared to the remaining terms, should be kept for comparison with the diagrammatic result.

The full two-loop corrections to $m_h^2$ at $\mathcal{O}(m_t^2h_t^4)$ have not yet been calculated in the diagrammatic approach; thus we neglect terms of this order in what follows. [3] With a slight rewriting of Eq. (23) we finally obtain the expression that will be compared with the diagrammatic result in the following sections:

$$m_h^2 = m_h^{2,\text{tree}} + \frac{3}{2}\frac{G_F\sqrt{2}}{\pi^2}\overline{m}_t^4\left\{-\ln\left(\frac{\overline{m}_t^2}{\overline{M}_S^2}\right) + \frac{\overline{X}_t^2}{\overline{M}_S^2}\left(1 - \frac{1}{12}\frac{\overline{X}_t^2}{\overline{M}_S^2}\right)\right\} - 3\frac{G_F\sqrt{2}}{\pi^2}\frac{\alpha_s}{\pi}\overline{m}_t^4\left\{\ln^2\left(\frac{\overline{m}_t^2}{\overline{M}_S^2}\right) + \left[\frac{2}{3} - 2\frac{\overline{X}_t^2}{\overline{M}_S^2}\left(1 - \frac{1}{12}\frac{\overline{X}_t^2}{\overline{M}_S^2}\right)\right]\ln\left(\frac{\overline{m}_t^2}{\overline{M}_S^2}\right)\right\}, \tag{24}$$

where we have introduced the notation $\overline{M}_S, \overline{X}_t$ to emphasize that the corresponding quantities are $\overline{\text{MS}}$ parameters, which are evaluated at the scale $\mu = M_S$:

$$\overline{M}_S \equiv M_S^{\overline{\text{MS}}}(M_S), \qquad \overline{X}_t \equiv X_t^{\overline{\text{MS}}}(M_S), \tag{25}$$

and $\overline{m}_t \equiv m_{t,\text{SM}}^{\overline{\text{MS}}}(m_t)$ as defined in Eq. (3).

## 3. Diagrammatic calculation

In the diagrammatic approach the masses of the $\mathcal{CP}$-even Higgs bosons are obtained by evaluating loop corrections to the $h$, $H$ and $hH$-mixing propagators. The masses of the

[2] In the "leading $m_t^4$ approximation" that is employed here, there is no distinction between $m_h(\overline{m}_t)$ and the on-shell (or pole) Higgs mass, $m_h$.

[3] As noted below Eq. (23), terms of $\mathcal{O}(m_t^2h_t^4)$ can be as numerically important as terms of $\mathcal{O}(m_t^2h_t^2\alpha_s)$. Hence, in a complete phenomenological analysis, one should not neglect terms of the former type.

two $\mathcal{CP}$-even Higgs bosons, $m_h$ and $m_H$, are determined as the poles of this propagator matrix, which are given by the solution of

$$\left[q^2 - m_h^{2,\text{tree}} + \widehat{\Sigma}_{hh}(q^2)\right]\left[q^2 - m_H^{2,\text{tree}} + \widehat{\Sigma}_{HH}(q^2)\right] - \left[\widehat{\Sigma}_{hH}(q^2)\right]^2 = 0, \tag{26}$$

where $\widehat{\Sigma}_{hh}(q^2)$, $\widehat{\Sigma}_{HH}(q^2)$ and $\widehat{\Sigma}_{hH}(q^2)$ denote the renormalized Higgs boson self-energies. In Ref. [17] the dominant two-loop contributions to the masses of the $\mathcal{CP}$-even Higgs bosons of $\mathcal{O}(\alpha\alpha_s)$ have been evaluated. These corrections, obtained in the on-shell scheme, have been combined in Refs. [18] and [19] with the complete one-loop on-shell result of Ref. [8] and the two-loop corrections of $\mathcal{O}(m_t^2 h_t^4)$ given in Refs. [13–15].

The diagrammatic two-loop calculation of Ref. [17] involves a renormalization in the Higgs sector up to the two-loop level and a renormalization in the stop sector up to $\mathcal{O}(\alpha_s)$. In the on-shell scheme, the renormalization in the stop sector is performed such that the $\tilde{t}$-masses $m_{\tilde{t}_1}$ and $m_{\tilde{t}_2}$ correspond to the poles of the propagators, i.e.:

$$\text{Re}\,\widehat{\Sigma}_{\tilde{t}_1\tilde{t}_1}\left(m_{\tilde{t}_1}^2\right) = 0, \qquad \text{Re}\,\widehat{\Sigma}_{\tilde{t}_2\tilde{t}_2}\left(m_{\tilde{t}_2}^2\right) = 0 \tag{27}$$

for the renormalized self-energies. In Ref. [17] the renormalization condition

$$\text{Re}\,\widehat{\Sigma}_{\tilde{t}_1\tilde{t}_2}\left(m_{\tilde{t}_1}^2\right) = 0 \tag{28}$$

has been chosen to define the stop mixing angle.[4] In Ref. [20] a compact analytic approximation has been derived from the rather complicated diagrammatic two-loop result by performing an expansion in $\Delta_{\tilde{t}}$ (Eq. (13)) of the $t$–$\tilde{t}$ sector contributions.

The diagrammatic two-loop corrections to the Higgs mass also depend nontrivially on the gluino mass, which is a free input parameter of the supersymmetric model. In the EFT approach described in Section 2, the gluino is decoupled at the same scale as the stops. Thus, in order to compare the results of the EFT and diagrammatic approaches, one must take $m_{\tilde{g}} \simeq \mathcal{O}(M_S)$. In this paper, we have chosen

$$m_{\tilde{g}} = M_{\text{SUSY}} = \sqrt{M_S^2 - m_t^2}. \tag{29}$$

For the one-loop contributions from the other sectors of the MSSM the leading logarithmic approximation has been used [11,15]. In this approximation, the momentum dependence in Eq. (26) is neglected everywhere. The resulting expression can thus be written as a correction to the tree-level mass matrix (Eq. (1)). The expression for $m_h^2$ in this approximation is obtained by diagonalizing the loop-corrected mass matrix. The compact analytic expression derived in this way, which is valid for arbitrary values of $m_A$, has been shown to approximate the full diagrammatic result for $m_h$ rather well, typically within about 2 GeV for most parts of the MSSM parameter space [20].

In the following we will restrict ourselves to the contribution of the $t$–$\tilde{t}$ sector. In order to perform a simple comparison with the EFT approach of Section 2, we only consider

[4] In this paper, our analysis is presented in a simplified model of stop mixing, where the tree-level stop squared-mass matrix given by Eq. (6). In this case, $\tilde{t}_1$ and $\tilde{t}_2$ are states of definite parity at tree-level. Since parity is preserved to all orders in $\alpha_s$, it follows that $\widehat{\Sigma}_{\tilde{t}_1\tilde{t}_2}(p^2) = 0$ (when electroweak corrections are neglected) and Eq. (28) is trivially satisfied.

the dominant one-loop and two-loop terms of $\mathcal{O}(m_t^2 h_t^2)$ and $\mathcal{O}(m_t^2 h_t^2 \alpha_s)$, respectively. We focus on the case $m_A \gg m_Z$, for which the result for $m_h^2$ can be expressed in a particularly compact form,

$$m_h^2 = m_h^{2,\text{tree}} + m_h^{2,\alpha} + m_h^{2,\alpha\alpha_s}, \tag{30}$$

and neglect the nonleading terms of $\mathcal{O}(m_Z^2/m_A^2)$. Moreover, assuming that $M_S \gg M_t$ and neglecting the nonleading terms of $\mathcal{O}(M_t/M_S)$ and $\mathcal{O}(m_Z^2/M_t^2)$, one obtains the following simple result for the one-loop and two-loop contributions:

$$m_h^{2,\alpha} = \frac{3}{2}\frac{G_F\sqrt{2}}{\pi^2} M_t^4 \left\{ -\ln\left(\frac{M_t^2}{M_S^2}\right) + \frac{X_t^2}{M_S^2}\left(1 - \frac{1}{12}\frac{X_t^2}{M_S^2}\right)\right\}, \tag{31}$$

$$m_h^{2,\alpha\alpha_s} = -3\frac{G_F\sqrt{2}}{\pi^2}\frac{\alpha_s}{\pi} M_t^4 \left\{ \ln^2\left(\frac{M_t^2}{M_S^2}\right) - \left(2 + \frac{X_t^2}{M_S^2}\right)\ln\left(\frac{M_t^2}{M_S^2}\right) - \frac{X_t}{M_S}\left(2 - \frac{1}{4}\frac{X_t^3}{M_S^3}\right)\right\}. \tag{32}$$

The corresponding formulae, in which terms up to $\mathcal{O}(M_t^4/M_S^4)$ are kept, can be found in Appendix B (see Eqs. (B.1) and (B.2)).

In Eqs. (31) and (32) the parameters $M_t$, $M_S$ and $X_t$ are on-shell quantities. Using Eq. (3), the on-shell result for $m_h^2$ (Eqs. (30)–(32)) can easily be rewritten in terms of the running top-quark mass $\overline{m}_t$. While this reparameterization does not change the form of the one-loop result, it induces an extra contribution at $\mathcal{O}(\alpha\alpha_s)$. Keeping again only terms that are not suppressed by powers of $\overline{m}_t/M_S$, the resulting expressions read

$$m_h^{2,\alpha} = \frac{3}{2}\frac{G_F\sqrt{2}}{\pi^2}\overline{m}_t^4 \left\{ -\ln\left(\frac{\overline{m}_t^2}{M_S^2}\right) + \frac{X_t^2}{M_S^2}\left(1 - \frac{1}{12}\frac{X_t^2}{M_S^2}\right)\right\}, \tag{33}$$

$$m_h^{2,\alpha\alpha_s} = -3\frac{G_F\sqrt{2}}{\pi^2}\frac{\alpha_s}{\pi}\overline{m}_t^4 \left\{ \ln^2\left(\frac{\overline{m}_t^2}{M_S^2}\right) + \left(\frac{2}{3} - \frac{X_t^2}{M_S^2}\right)\ln\left(\frac{\overline{m}_t^2}{M_S^2}\right) + \frac{4}{3} - 2\frac{X_t}{M_S} - \frac{8}{3}\frac{X_t^2}{M_S^2} + \frac{17}{36}\frac{X_t^4}{M_S^4}\right\}, \tag{34}$$

in accordance with the formulae given in Ref. [20].

We now compare the diagrammatic result expressed in terms of the parameters $\overline{m}_t$, $M_S$ and $X_t$ (Eqs. (33) and (34)) with the EFT result (Eq. (24)) which is given in terms of the $\overline{\text{MS}}$ parameters $\overline{m}_t$, $\overline{M}_S$ and $\overline{X}_t$ (Eq. (25)). While the $X_t$-independent logarithmic terms are the same in both the diagrammatic and EFT results, the corresponding logarithmic terms at two-loops that are proportional to powers of $X_t$ and $\overline{X}_t$, respectively, are different. Furthermore, Eq. (34) does not contain a logarithmic term proportional to $X_t^4$, while the corresponding term proportional to $\overline{X}_t^4$ appears in Eq. (24). To check whether these results are consistent, one must relate the on-shell and $\overline{\text{MS}}$ definitions of the parameters $M_S$ and $X_t$.

Finally, we note that the nonlogarithmic terms contained in Eq. (34) correspond to genuine two-loop contributions that are not present in the EFT result of Eq. (24). They can

be interpreted as a two-loop finite threshold correction to the quartic Higgs self-coupling in the EFT approach. In particular, note that Eq. (34) contains a term that is linear in $X_t$ This is the main source of the asymmetry in the two-loop corrected Higgs mass under $X_t \to -X_t$ obtained by the diagrammatic method. The nonlogarithmic terms in Eq. (34) give rise to a numerically significant increase of the maximal value of $m_h$ of about 5 GeV in this approximation.

## 4. On-shell and $\overline{\rm MS}$ definitions of $M_S$ and $X_t$

Since the parameters $p = \{m^2_{\tilde{t}_1}, m^2_{\tilde{t}_2}, \theta_{\tilde{t}}, m_t\}$ of the $t$–$\tilde{t}$ sector are renormalized differently in different schemes, the parameters $M_S$ and $X_t$ also have a different meaning in these schemes. In order to derive the relation between these parameters in the $\overline{\rm MS}$ and in the on-shell scheme we start from the observation that at lowest order the parameters $p$ are the same in both schemes, i.e., $p = p^{\rm OS} = p^{\overline{\rm MS}}$ in lowest order. Expressing the bare parameters in terms of the renormalized parameters and the counterterms leads to

$$p^{\overline{\rm MS}} + \delta p^{\overline{\rm MS}} = p^{\rm OS} + \delta p^{\rm OS}. \tag{35}$$

Here $\delta p^{\rm OS}$ is the on-shell counterterm in $D \equiv 4 - 2\varepsilon$ dimensions, and according to the $\overline{\rm MS}$ prescription $\delta p^{\overline{\rm MS}}$ is given just by the pole part of $\delta p^{\rm OS}$, i.e., the contribution proportional to $1/\varepsilon - \gamma_{\rm E} + \ln 4\pi$, where $\gamma_{\rm E}$ is Euler's constant. The $\overline{\rm MS}$ parameters are thus related to the on-shell parameters by

$$p^{\overline{\rm MS}} = p^{\rm OS} + \Delta p, \tag{36}$$

where $\Delta p \equiv \delta p^{\rm OS} - \delta p^{\overline{\rm MS}}$ is finite in the limit $D \to 4$ and contains the $\overline{\rm MS}$ scale $\mu$ which can be chosen appropriately. In this paper, we only need to know $\Delta p$ to $\mathcal{O}(\alpha_s)$ one-loop accuracy. In the following we will compare the result for $m_h$ expressed in terms of the on-shell parameters $p^{\rm OS}$ with results for $m_h$ in terms of the corresponding $\overline{\rm MS}$ parameters $p^{\overline{\rm MS}}$, which are related to $p^{\rm OS}$ as in Eq. (36).

In the EFT approach, the parameters $M_S$ and $X_t$ are running parameters evaluated at the scale $\mu = M_S$ (Eq. (25)). In the simplified model for the stop squared-mass matrix given by Eq. (6), the relations between the parameters $X_t$ and $M_S$ in the on-shell and $\overline{\rm MS}$ scheme are obtained using

$$m^{2,{\rm OS}}_{\tilde{t}_1} = M_S^{2,{\rm OS}} \mp M_t X_t^{\rm OS}, \qquad m^{2,{\rm OS}}_{\tilde{t}_2} = M_S^{2,{\rm OS}} \pm M_t X_t^{\rm OS}, \tag{37}$$

$$m^{2,\overline{\rm MS}}_{\tilde{t}_1} = \overline{M}_S^2 \mp \overline{m}_t(M_S)\overline{X}_t, \qquad m^{2,\overline{\rm MS}}_{\tilde{t}_2} = \overline{M}_S^2 \pm \overline{m}_t(M_S)\overline{X}_t, \tag{38}$$

where we have written $\overline{m}_t(M_S) \equiv m_t^{\overline{\rm MS}}(M_S)$ and $M_t \equiv m_t^{\rm OS}$ as in Section 2. In both Eqs. (37) and (38), the upper and lower signs refer to $X_t^{\rm OS} > 0$ and $X_t^{\rm OS} < 0$, respectively. In the model of stop mixing under consideration, there is no shift in the scalar top mixing angle to all orders in $\alpha_s$, from which it follows that $|\theta^{\rm OS}_{\tilde{t}}| = |\theta^{\overline{\rm MS}}_{\tilde{t}}|$.

Inserting the relation between $m^2_{\tilde{t}_1}$ and $m^2_{\tilde{t}_2}$ in the on-shell and the $\overline{\rm MS}$ scheme into Eqs. (37) and (38) yields up to first order in $\alpha_s$:

$$\overline{M}_S^2 = M_S^{2,\mathrm{OS}} + \tfrac{1}{2}\big(\Delta m^2_{\tilde{t}_1} + \Delta m^2_{\tilde{t}_2}\big), \tag{39}$$

$$\overline{X}_t = X_t^{\mathrm{OS}} \frac{M_t}{\overline{m}_t(M_S)} \pm \frac{1}{2m_t}\big(\Delta m^2_{\tilde{t}_2} - \Delta m^2_{\tilde{t}_1}\big), \tag{40}$$

where again the upper and lower sign in the last equation refers to $X_t^{\mathrm{OS}} > 0$ and $X_t^{\mathrm{OS}} < 0$, respectively. In the second term of Eq. (40) it is not necessary to distinguish (at one-loop) between $\overline{m}_t(M_S)$ and $M_t$, since $\Delta m^2_{\tilde{t}_1}$ and $\Delta m^2_{\tilde{t}_2}$ are $\mathcal{O}(\alpha_s)$ quantities; hence, the generic symbol $m_t$ is used here.

In Appendix A, we have obtained explicit results for $\Delta m^2_{\tilde{t}_1}$, $\Delta m^2_{\tilde{t}_2}$ and $M_t/\overline{m}_t(M_S)$. Inserting the appropriate expressions for these quantities into Eq. (40), one observes that the functional form for $\overline{X}_t$ is the same for $X_t^{\mathrm{OS}} > 0$ and $X_t^{\mathrm{OS}} < 0$ (i.e., the sign difference in Eq. (40) is compensated by the term $\big(\Delta m^2_{\tilde{t}_2} - \Delta m^2_{\tilde{t}_1}\big)$). As a result, it is no longer necessary to distinguish between these two cases. The case $X_t^{\mathrm{OS}} = 0$ (which formally would have to be treated separately) is understood as being included in Eq. (40).

Using the expansions given in Appendix A and setting the gluino mass according to Eq. (29), we obtain to leading order in $m_t/M_S$:

$$\overline{M}_S^2 = M_S^{2,\mathrm{OS}} - \frac{8}{3}\frac{\alpha_s}{\pi} M_S^2, \tag{41}$$

$$\overline{X}_t = X_t^{\mathrm{OS}} \frac{M_t}{\overline{m}_t(M_S)} + \frac{8}{3}\frac{\alpha_s}{\pi} M_S. \tag{42}$$

As previously noted, it is not necessary to specify the definition of the parameters that appear in the $\mathcal{O}(\alpha_s)$ terms. Thus, we use the generic symbol $M_S^2$ in the $\mathcal{O}(\alpha_s)$ terms of Eqs. (41)–(42). The corresponding results including terms up to $\mathcal{O}\big(m_t^4/M_S^4\big)$ can be found in Appendix B.

Finally, we need to evaluate the ratio $M_t/\overline{m}_t(M_S)$. The relevant expression is given in Eq. (A.14). Using the expansions given at the end of Appendix A, we find to leading order in $m_t/M_S$:

$$\overline{m}_t(M_S) = \overline{m}_t\left[1 + \frac{\alpha_s}{\pi}\ln\left(\frac{m_t^2}{M_S^2}\right) + \frac{\alpha_s}{3\pi}\frac{X_t}{M_S}\right], \tag{43}$$

where $\overline{m}_t \equiv m_{t,\mathrm{SM}}^{\overline{\mathrm{MS}}}(m_t)$ is given in terms of $M_t$ by Eq. (3). The corresponding formula, where terms up to $\mathcal{O}(m_t^4/M_S^4)$ are kept, can be found at the end of Appendix B. Note that the term in Eq. (43) that is proportional to $X_t$ is a threshold correction due to the supersymmetry-breaking stop-mixing effect. Inserting the result of Eq. (43) into Eq. (42) yields:

$$\overline{X}_t = X_t^{\mathrm{OS}} + \frac{\alpha_s}{3\pi} M_S\left[8 + \frac{4X_t}{M_S} - \frac{X_t^2}{M_S^2} - \frac{3X_t}{M_S}\ln\left(\frac{m_t^2}{M_S^2}\right)\right]. \tag{44}$$

It is interesting to note that $\overline{X}_t \neq 0$ when $X_t^{\mathrm{OS}} = 0$. Moreover, it is clear from Eq. (44) that the relation between $X_t$ defined in the on-shell and the $\overline{\mathrm{MS}}$ schemes includes a leading logarithmic effect, which has to be taken into account in a comparison of the leading logarithmic contributions in the EFT and the two-loop diagrammatic results.

The above results are relevant for calculations in the full theory in which the effects of the supersymmetric particles are fully taken into account. However, in effective field theory below $M_S$, one must decouple the supersymmetric particles from the loops and compute with the standard model spectrum. Thus, it will be useful to define a running $\overline{\rm MS}$ top-quark mass in the effective standard model, $m_{t,\rm SM}^{\overline{\rm MS}}(\mu)$, which to $\mathcal{O}(\alpha_s)$ is given by:

$$m_{t,\rm SM}^{\overline{\rm MS}}(\mu) = \overline{m}_t\left[1 + \frac{\alpha_s}{\pi}\ln\left(\frac{m_t^2}{\mu^2}\right)\right]. \tag{45}$$

At the scale $M_S$, we must match this result onto the expression for $\overline{m}_t(M_S)$ as computed in the full theory (Eq. (43)). The matching is discontinuous at $\mu = M_S$ due to the threshold corrections arising from stop mixing effects.

In comparing with the EFT results of Refs. [12–15], it should be noted that the threshold correction in Eq. (43) were omitted. This is relevant, since $\overline{m}_t(M_S)$ (or the related quantity $h_t(M_S)$, see Eq. (11)) appears in the threshold correction to the quartic Higgs self-coupling $\lambda(M_S)$ (Eqs. (9) and (10)). In Refs. [12–15], $\overline{m}_t(M_S)$ is reexpressed in terms of $\overline{m}_t(m_t)$ by using Eq. (45) rather than Eq. (43). As a result, a two-loop non-logarithmic term proportional to $X_t$ is missed in the computation of $m_h$. Such a term is of the same order as the two-loop threshold correction to the quartic Higgs self-coupling, which were also neglected in Refs. [12–15]. However, in this work we do not neglect the latter. Hence, it would be incorrect to use Eq. (45) in the evaluation of $\overline{m}_t(M_S)$. In Section 5 we will apply $\overline{m}_t(\mu)$ with different choices of $\mu$ for the $X_t$-independent and $X_t$-dependent contributions to $m_h^2$, which will prove useful for absorbing numerically large two-loop contributions into an effective one-loop result. In the spirit of EFT, we will argue that for $\mu = M_S$, one should use the results of Eq. (43) while for $\mu < M_S$, one should use Eq. (45).

A remark on the regularization scheme is in order here. In effective field theory, the running top-quark mass at scales below $M_S$ is the SM running coupling (Eq. (45)), which is calculated in dimensional regularization. This is matched onto the running top-quark mass as computed in the full supersymmetric theory. One could argue that the appropriate regularization scheme for the latter should be dimensional reduction (DRED) [26,27], which is usually applied in loop calculations in supersymmetry.[5] The result of such a change would be to modify slightly the two-loop non-logarithmic contribution to $m_h$ that is proportional to powers of $X_t$. Of course, the physical Higgs mass is independent of scheme. One is free to reexpress Eqs. (31) and (32) (which depend on the on-shell parameters $M_t$, $M_S$, $X_t$) in terms of parameters defined in any other scheme. In this paper, we find $\overline{\rm MS}$-renormalization via DREG to be the most convenient scheme for the comparison of the diagrammatic and EFT results for $m_h$.

[5] In order to obtain the corresponding DRED result, one simply has to replace the term $4\alpha_s/3\pi$ in the denominator of Eq. (3) by $5\alpha_s/3\pi$.

## 5. Comparing the EFT and diagrammatic results

In order to directly compare the two-loop diagrammatic and EFT results, we must convert from on-shell to $\overline{\rm MS}$ parameters. Inserting Eqs. (41) and (44) into Eqs. (33) and (34), one finds

$$m_h^{2,\alpha} = \frac{3}{2}\frac{G_F\sqrt{2}}{\pi^2}\overline{m}_t^4\left\{-\ln\left(\frac{\overline{m}_t^2}{\overline{M}_S^2}\right)+\frac{\overline{X}_t^2}{\overline{M}_S^2}\left(1-\frac{1}{12}\frac{\overline{X}_t^2}{\overline{M}_S^2}\right)\right\}, \tag{46}$$

$$\begin{aligned} m_h^{2,\alpha\alpha_s} = {} & -3\frac{G_F\sqrt{2}}{\pi^2}\frac{\alpha_s}{\pi}\overline{m}_t^4\left\{\ln^2\left(\frac{\overline{m}_t^2}{\overline{M}_S^2}\right)+\left[\frac{2}{3}-2\frac{\overline{X}_t^2}{\overline{M}_S^2}\left(1-\frac{1}{12}\frac{\overline{X}_t^2}{\overline{M}_S^2}\right)\right]\ln\left(\frac{\overline{m}_t^2}{\overline{M}_S^2}\right)\right. \\ & \left.+\frac{\overline{X}_t}{\overline{M}_S}\left(\frac{2}{3}-\frac{7}{9}\frac{\overline{X}_t^2}{\overline{M}_S^2}+\frac{1}{36}\frac{\overline{X}_t^3}{\overline{M}_S^3}+\frac{1}{18}\frac{\overline{X}_t^4}{\overline{M}_S^4}\right)\right\} \\ & +\mathcal{O}\left(\frac{\overline{m}_t}{\overline{M}_S}\right). \end{aligned} \tag{47}$$

Comparing Eq. (47) with Eq. (24) shows that the logarithmic contributions of the diagrammatic result expressed in terms of the $\overline{\rm MS}$ parameters $\overline{m}_t$, $\overline{M}_S$ and $\overline{X}_t$ agree with the logarithmic contributions obtained by the EFT approach. The differences in the logarithmic terms observed in the comparison of Eqs. (33) and (34) with Eq. (24) have thus been traced to the different renormalization schemes applied in the respective calculations. The fact that the logarithmic contributions obtained within the two approaches agree after a proper rewriting of the parameters of the stop sector is an important consistency check of the calculations. In addition to the logarithmic contributions, Eq. (47) also contains nonlogarithmic contributions, which are numerically sizable.

In Fig. 1, we compare the diagrammatic result for $m_h$ in the leading $m_t^4$ approximation to the results obtained in Section 2 by EFT techniques, for two different values of $\tan\beta$. However, as noted at the end of Section 4, in the derivation of the EFT result of Eq. (24) the supersymmetric threshold corrections to $\overline{m}_t(M_S)$ were neglected. Thus $\overline{X}_t$ which appears in Eqs. (46) and (47) is not precisely the same as the $\overline{X}_t$ parameter appearing in the EFT result of Eq. (24) due to the difference in the definition of $\overline{m}_t(M_S)$ (Eq. (43)) and $m_{t,\rm SM}^{\overline{\rm MS}}$ (Eq. (45)). Taking this difference into account in Eq. (42), it follows that the $\overline{X}_t$ parameter that appears in Eq. (24) is given by $\overline{X}_t' \equiv \overline{X}_t\,[1+(\alpha_s/3\pi)(X_t/M_S)]$. It can be easily checked that the change from $\overline{X}_t$ to $\overline{X}_t'$ does not affect the comparison of two-loop logarithmic terms between Eqs. (24) and (47). Moreover, the difference between $\overline{X}_t$ and $\overline{X}_t'$ is numerically small. In Fig 1, the diagrammatic result for $m_h$ is plotted versus $\overline{X}_t$, while the EFT result is plotted versus $\overline{X}_t'$.

While the diagrammatic result expressed in terms of $\overline{m}_t$, $\overline{M}_S$, $\overline{X}_t$ agrees well with the EFT result in the region of no mixing in the stop sector, sizable deviations occur for large mixing. In particular, the nonlogarithmic contributions give rise to an asymmetry under the change of sign of the parameter $\overline{X}_t$, while the EFT result is symmetric under $\overline{X}_t \to -\overline{X}_t$. In the approximation considered here, the maximal value for $m_h$ in the diagrammatic result lies about 3 GeV higher than the maximal value of the EFT result for $\tan\beta = 1.6$. The differences are slightly smaller for $\tan\beta = 30$. In addition, as previously noted, the

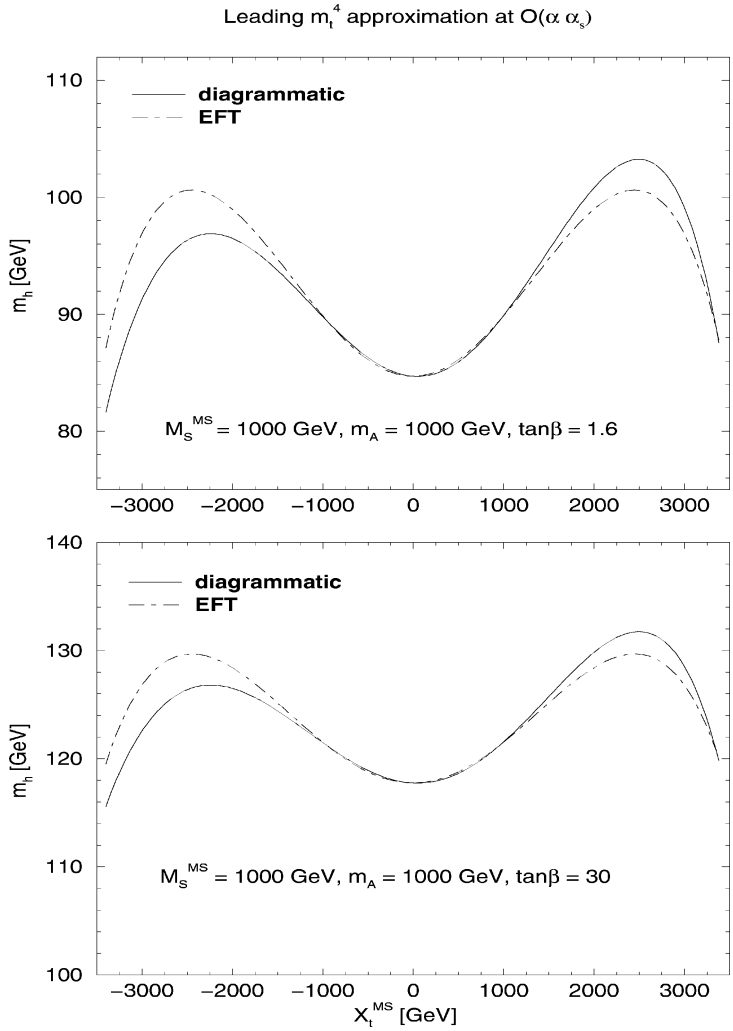


Fig. 1. Comparison of the diagrammatic two-loop $\mathcal{O}(m_t^2 h_t^2 \alpha_s)$ result for $m_h$, to leading order in $\overline{m}_t/\overline{M}_S$ (Eqs. (46) and (47)) with the EFT result of Eq. (24). Note that the latter omits the one-loop threshold corrections due to stop mixing in the evaluation of $\overline{m}_t(M_S)$. Since this quantity enters in the definition of $\overline{X}_t$ (see Eq. (42)), the meaning of $X_t^{\rm MS}$ plotted along the $x$-axis is slightly different for the diagrammatic curve, where $X_t^{\rm MS} = \overline{X}_t$, and the EFT curve, where $X_t^{\rm MS} = \overline{X}_t\,[1 + (\alpha_s/3\pi)(X_t/M_S)]$. See text for further details. The two graphs above are plotted for $\overline{M}_S = m_A = (m_{\tilde{g}}^2 + \overline{m}_t^2)^{1/2} = 1$ TeV for the cases of $\tan\beta = 1.6$ and $\tan\beta = 30$, respectively.

maximal-mixing point $(\overline{X}_t)_{\rm max}$ (where the radiatively corrected value of $m_h$ is maximal) is equal to its one-loop value, $(\overline{X}_t)_{\rm max} \simeq \pm\sqrt{6}M_S$, in the EFT result of Eq. (24), while it is shifted in the two-loop diagrammatic result. However, Fig. 1 illustrates that the shift in $(\overline{X}_t)_{\rm max}$ from its one-loop value, while significant in the two-loop on-shell diagrammatic result, is largely diminished when the latter is reexpressed in terms of $\overline{\rm MS}$ parameters.

The differences between the diagrammatic and EFT results shown in Fig. 1 can be attributed to nonnegligible nonlogarithmic terms proportional to powers of $X_t$. Clearly, the EFT technique can be improved to incorporate these terms. As previously discussed, one can account for such terms in the EFT approach by: (i) including one-loop finite threshold effects in the definition of $\overline{m}_t(M_S)$, and (ii) including two-loop finite threshold effects to $\Delta_{\rm th}\lambda$ (Eq. (10)) in the matching condition for $\lambda(M_S)$.[6] Although both effects are nominally of the same order, it is interesting to investigate what fraction of the terms proportional to powers of $\overline{X}_t$ in Eq. (47) can be obtained by including the threshold effects in the definition of $\overline{m}_t(M_S)$.

In Ref. [15], it was shown that the leading two-loop contributions to $m_h^2$ given by the EFT result of Eq. (24) could be absorbed into an effective one-loop expression. This was accomplished by considering separately the $X_t$-independent leading double logarithmic term (the "no-mixing" contribution) and the leading single logarithmic term that is proportional to powers of $\overline{X}_t$ (the "mixing" contribution) at $\mathcal{O}(m_t^2 h_t^2 \alpha_s)$. Both terms can be reproduced by an effective one-loop expression, where $\overline{m}_t$ in Eq. (46), which appears in the no-mixing and mixing contributions, is replaced by the *running* top-quark mass evaluated at the scales $\mu_t$ and $\mu_{\tilde{t}}$, respectively:

$$\text{no-mixing:}\quad \mu_t \equiv \left(\overline{m}_t \overline{M}_S\right)^{1/2}, \qquad \text{mixing:}\quad \mu_{\tilde{t}} \equiv \overline{M}_S. \tag{48}$$

That is, at $\mathcal{O}(m_t^2 h_t^2 \alpha_s)$, the leading double logarithmic term is precisely reproduced by the single-logarithmic term at $\mathcal{O}(m_t^2 h_t^2)$, by replacing $\overline{m}_t$ with $\overline{m}_t(\mu_t)$, while the leading single logarithmic term at two-loops proportional to powers of $\overline{X}_t$ is precisely reproduced by the corresponding nonlogarithmic terms proportional to $\overline{X}_t$ at $\mathcal{O}(m_t^2 h_t^2)$, by replacing $\overline{m}_t$ with $\overline{m}_t(\overline{M}_S)$.

Applying the same procedure to Eq. (47) and rewriting it in terms of the running top-quark mass at the corresponding scales as specified in Eq. (48), we obtain:

$$m_h^{2,\alpha} = \frac{3}{2}\frac{G_F\sqrt{2}}{\pi^2}\left\{-\overline{m}_t^4(\mu_t)\ln\left(\frac{\overline{m}_t^2(\mu_t)}{\overline{M}_S^2}\right) + \overline{m}_t^4(\overline{M}_S)\frac{\overline{X}_t^2}{\overline{M}_S^2}\left(1 - \frac{\overline{X}_t^2}{12\overline{M}_S^2}\right)\right\}, \tag{49}$$

$$m_h^{2,\alpha\alpha_s} = -3\frac{G_F\sqrt{2}}{\pi^2}\frac{\alpha_s}{\pi}m_t^4\left\{\frac{1}{6}\ln\left(\frac{m_t^2}{M_S^2}\right) + \frac{X_t}{M_S}\left(\frac{2}{3} - \frac{1}{9}\frac{{X_t}^2}{M_S^2} + \frac{1}{36}\frac{{X_t}^3}{M_S^3}\right)\right\}. \tag{50}$$

Indeed, the $X_t$-independent leading double logarithmic term and the leading single logarithmic term that is proportional to powers of $\overline{X}_t$ have disappeared from the two-loop expression (Eq. (50)), having been absorbed into an effective one-loop result (Eq. (49)) (denoted henceforth as the "mixed-scale" one-loop EFT result). Of the terms that remain (Eq. (50)), there is a subleading one-loop logarithm at two-loops which is a remnant of the no-mixing contribution. But, note that the magnitude of the coefficient (1/6) has been reduced from the corresponding coefficients that appear in Eqs. (32) and (47) ($-2$ and

[6] An additional two-loop $\mathcal{O}(h_t^2\alpha_s)$ correction to $\lambda(M_S)$ can arise because the Higgs self-coupling in the $\overline{\rm MS}$ scheme does not precisely satisfy the supersymmetric relation $\lambda(M_S) = \frac{1}{4}(g^2 + g'^2)\cos^2 2\beta$ in the supersymmetric limit. This correction corresponds to a matching of the $\overline{\rm MS}$ and $\overline{\rm DR}$ couplings at the scale $M_S$ [28]. We will count this as part of the two-loop finite threshold effects.

2/3, respectively). In addition, the remaining leftover two-loop nonlogarithmic terms are also numerically insignificant. We conclude that the "mixed-scale" one-loop EFT result provides a very good approximation to $m_h^2$, in which the most significant two-loop terms have been absorbed into an effective one-loop expression.

To illustrate this result, we compare in Fig. 2 the diagrammatic two-loop result expressed in terms of $\overline{\rm MS}$ parameters (Eqs. (46) and (47)) with the "mixed-scale" one-loop EFT result (Eq. (49)) as a function of $\overline{X}_t$. In order to make a fair comparison of two-loop expressions, we first evaluate Eq. (49) as a perturbation expansion which is truncated beyond the $\mathcal{O}(\alpha_s^2)$ term.[7] It is this result that is plotted as a dashed line in Fig. 2. Note that by construction, the sum of the two-loop truncated version of Eq. (49) and the leftover two-loop term given by Eq. (50) is equal to the sum of Eqs. (46) and (47). That is, the difference between the solid and dashed lines of Fig. 2 is precisely equal to the leftover two-loop term given by Eq. (50), which is seen to be numerically small. Hence, within the simplifying framework under consideration (i.e., only leading $t$–$\tilde{t}$ sector-contributions are taken into account assuming a simplified stop squared-mass matrix (Eq. (6)), with $\overline{M}_S$, $m_A \gg \overline{m}_t$ and $m_{\tilde{g}} = M_{\rm SUSY}$), we see that the "mixed-scale" one-loop result for $m_h$ provides a very good approximation to a more complete two-loop result for all values of $\overline{X}_t$.[8] In the EFT picture this means that, once reexpressed in terms of the appropriate $\overline{\rm MS}$ running parameters, the dominant contributions to the lightest $\mathcal{CP}$-even Higgs mass arising from the two-loop threshold corrections induced by the decoupling of the stops, have their origin in the one-loop threshold corrections to the Higgs–top quark Yukawa coupling.

In the present analysis we have focused on the leading contributions of the $t$–$\tilde{t}$ sector of the MSSM. However, these contributions alone are not sufficient to provide an accurate determination of the Higgs mass (and can be off by 5 GeV or more in certain regions of the MSSM parameter space). In any realistic phenomenological analysis of the properties of the Higgs sector, one must include sub-leading contributions of the $t$–$\tilde{t}$ sector as well as contributions from other particle/superpartner sectors. Such contributions have been obtained within the EFT approach in Refs. [14,15], which incorporates one-loop leading logarithmic terms from all partner/superpartner sectors, plus single and double logarithmic two-loop contributions from the $t$–$\tilde{t}$ and $b$–$\widetilde{b}$ sectors. The full one-loop diagrammatic result is known [7–9], and this along with the diagrammatic two-loop result from the $t$–$\tilde{t}$ sector at $\mathcal{O}(\alpha\alpha_s)$ are included in the Fortran code *FeynHiggs* [29]. The impact of the additional contributions to the radiatively-corrected Higgs mass on phenomenological studies have been investigated in Refs. [19,30].

In the large $\tan\beta$ regime, the $b$–$\widetilde{b}$ sector is especially important. Here the corrections induced by the bottom Yukawa coupling become relevant, and one should correspondingly

[7] For example, using Eq. (45), we would write $\overline{m}_t^4(\mu_t) = \overline{m}_t^4[1 + 4(\alpha_s/\pi)\ln(m_t^2/\mu_t^2)]$ and insert this into Eq. (49).

[8] Strictly speaking, the analytic approximations of this paper break down when $\overline{m}_t \overline{X}_t \sim \overline{M}_S^2$. Thus, one does not expect an accurate result for the corresponding formulae when $\overline{X}_t$ is too large [13,15,20]. In practice, one should not trust the accuracy of the analytic formulae once $\overline{X}_t > (\overline{X}_t)_{\rm max}$.

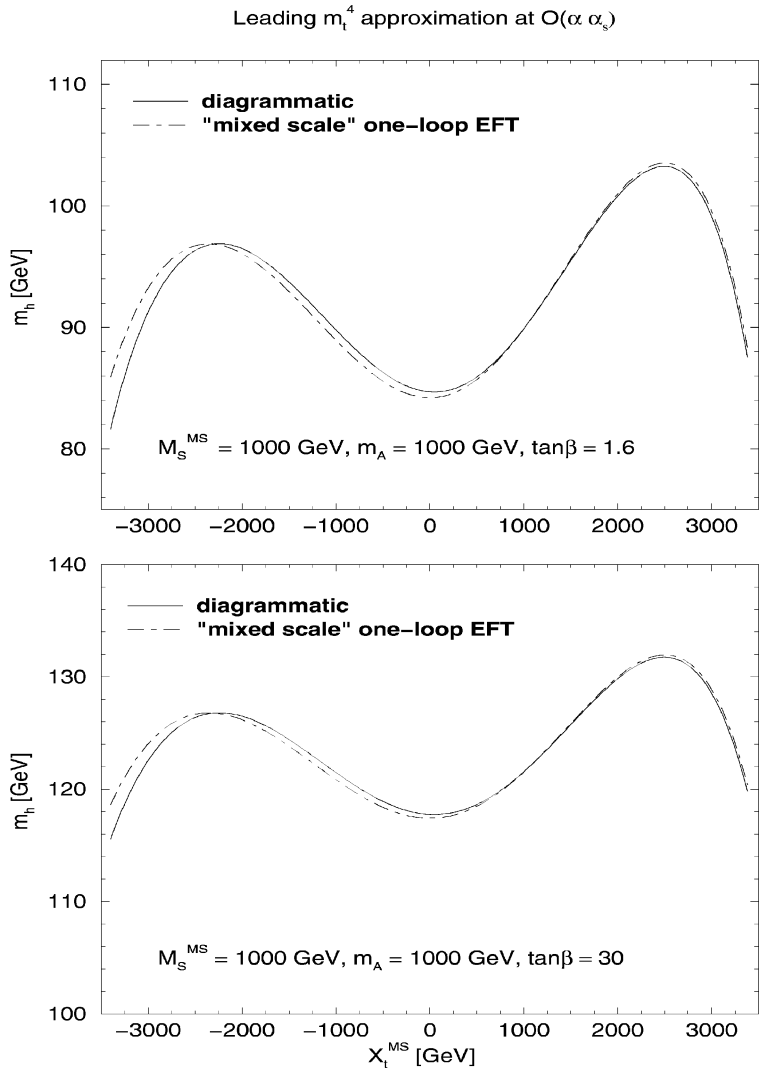


Fig. 2. Comparison of the diagrammatic two-loop $\mathcal{O}(m_t^2 h_t^2 \alpha_s)$ result for $m_h$, to leading order in $\overline{m}_t/\overline{M}_S$ (Eqs. (46) and (47)) with the "mixed-scale" one-loop EFT result (Eq. (49)). Note that the latter now includes the threshold corrections due to stop mixing in the evaluation of $\overline{m}_t(M_S)$ in contrast to the EFT results depicted in Fig. 1. "Mixed-scale" indicates that in the no-mixing and mixing contributions to the one-loop Higgs mass, the running top quark mass is evaluated at different scales according to Eq. (48). See text for further details. The two graphs above are plotted for $\overline{M}_S = m_A = (m_{\tilde{g}}^2 + \overline{m}_t^2)^{1/2} = 1$ TeV for the cases of $\tan\beta = 1.6$ and $\tan\beta = 30$, respectively.

include the bottom mass corrections originating from the decoupling of the supersymmetric particles. These corrections are enhanced by a large $\tan\beta$ factor and hence can have a sizable impact on the phenomenology of the Higgs sector. Some of the most relevant consequences of these corrections have been recently discussed in Refs. [31–37].

## 6. Discussion and conclusions

In this work, we have compared the results for the lightest $\mathcal{CP}$-even Higgs-boson mass obtained from the two-loop $\mathcal{O}(\alpha\alpha_s)$ diagrammatic calculation in the on-shell scheme with the results of an effective field theory approach. In the latter, the two-loop $\mathcal{O}(\alpha\alpha_s)$ terms are generated via renormalization group running of the effective low-energy parameters from the supersymmetry-breaking scale, $M_S$ to the scale $m_t$. We have focused on the leading $\mathcal{O}(m_t^2 h_t^2 \alpha_s)$ two-loop contributions to $m_h^2$ in the limit of large $m_A$ and $M_S$. In this case, the effective field theory below $M_S$ is the one-Higgs-doublet standard model, which greatly simplifies the calculation. In addition, the gluino mass was set to $m_{\tilde{g}} = M_{\rm SUSY} \equiv (M_S^2 - m_t^2)^{1/2}$. The resulting transparent analytic expressions for the radiatively-corrected Higgs mass were well suited for investigating the basic relations between the various approaches. In order to compare the on-shell diagrammatic and effective field theory approaches, one must note two important facts. First, the two calculations are performed in different renormalization schemes. Hence, the resulting expressions actually depend on soft-supersymmetry-breaking parameters whose definitions differ at the one-loop level. Second, the diagrammatic calculation includes genuine nonlogarithmic two-loop corrections to the lightest $\mathcal{CP}$-even Higgs-boson mass. In the effective field theory approach, these would correspond to two-loop threshold corrections resulting from the decoupling of the two heavy top squarks in the low energy effective theory.

Previous comparisons of the corresponding two-loop results revealed an apparent discrepancy between terms that depend logarithmically on $M_S$, and different dependences of the nonlogarithmic terms on $X_t$. However, after reexpressing the one-loop and the two-loop terms of the on-shell diagrammatic result in terms of $\overline{\rm MS}$ parameters, i.e., applying the same renormalization scheme for both approaches, we have shown that the discrepancy in the logarithmic dependence on $M_S$ of both expressions disappears. This constitutes an important consistency check of the calculations. There remain, however, genuine nonlogarithmic two-loop contributions in the diagrammatic result. They give rise to an asymmetry under $X_t \to -X_t$, while the effective field theory computations that neglected the two-loop threshold corrections due to stop mixing only yield results that are symmetric under the change of sign of $X_t$. Moreover, the nonlogarithmic two-loop contributions of the on-shell diagrammatic computation, in the approximations considered in this paper, can *increase* the predicted value of $m_h$ by as much as 3 GeV.[9] Finally, they induce a shift of the value of $X_t$ where $m_h$ is maximal relative to the corresponding one-loop value $(X_t)_{\rm max} \simeq \pm\sqrt{6} M_S$. It is interesting to note that this shift is more (less) pronounced when $m_h$ is expressed in terms of $X_t$ in the on-shell ($\overline{\rm MS}$) scheme. The effect of the leading nonlogarithmic two-loop contributions can be taken into account in the effective field theory method by incorporating the $\mathcal{O}(h_t^2\alpha_s)$ $X_t$-dependent corrections into the boundary conditions of the effective quartic Higgs self-coupling at the scale $M_S$ and

[9] If only the on-shell top-quark mass is reexpressed in terms of the corresponding $\overline{\rm MS}$ parameter, the resulting increase in $m_h$ can be as much as 5 GeV.

performing a proper one-loop $\mathcal{O}(\alpha_s)$ matching of the running Higgs–top Yukawa coupling at $M_S$.

In Ref. [15], it was shown that the leading two-loop contributions to $m_h^2$ could be absorbed into an effective one-loop expression by the following procedure. The running top-quark mass that appears in the $X_t$-independent one-loop expression for $m_h^2$ is evaluated at the scale $\mu_t = (M_S m_t)^{1/2}$. In the corresponding $X_t$-dependent terms, the running top quark mass is evaluated at the scale $\mu_{\tilde{t}} = M_S$. The result, which we call the *mixed-scale* one-loop EFT expression neatly incorporates the leading two-loop effects. In this paper, we have extended this result by explicitly including stop mixing effects in evaluating the running parameters $\overline{m}_t(M_S)$ and $h_t(M_S)$. By doing so, we are able to incorporate some portion of the genuine leading nonlogarithmic two-loop contributions. The remaining terms at this order would then be identified with two-loop threshold corrections to the effective Higgs quartic coupling at the scale $M_S$. Remarkably, the latter turn out to be numerically small. This means that the mixed-scale one-loop EFT expression for $m_h$ provides a rather accurate estimate of the radiatively-corrected mass of the lightest $\mathcal{CP}$-even Higgs boson of the MSSM.

The above results have been obtained in a rather simple setting. A special choice for the stop squared-mass matrix was made (Eq. (6)) to simplify our analysis. The gluino mass was fixed to a value of order $M_S$. The leading $\mathcal{O}(m_t^2 h_t^4)$ corrections were neglected. Subleading terms of $\mathcal{O}(m_Z^2 h_t^2 \alpha_s)$ and $\mathcal{O}(m_Z^2 h_t^4)$ terms were also neglected. For example, consider the effect of varying the gluino mass. The two-loop diagrammatic results of Refs. [17–20] showed that the value of $m_h$ changed by as much as $\pm 2$ GeV as a function of $m_{\tilde{g}}$, for $m_t \lesssim m_{\tilde{g}} \lesssim M_S$. The gluino mass dependence can be treated in the EFT approach as follows. Let us assume that $M_S$ characterizes the scale of the squark masses, and $m_{\tilde{g}} < M_S$. Then, at scales below $M_S$ one integrates out the squarks but keeps the gluino as part of the low-energy effective theory. However, since the gluino *always* appears with squarks in diagrams contributing to $m_h^2$ at two-loops, once the squarks are integrated out, they no longer affect the running of any of the relevant low-energy parameters below $M_S$. However, the gluino mass does affect the value of $h_t(M_S)$ and $\overline{m}_t(M_S)$ (the relevant formulae are given in Appendix A). Thus, in the EFT approach, gluino mass dependence enters via the threshold corrections to the Higgs–top quark Yukawa couplings.

The case of a more general stop squared-mass matrix can be treated using the same methods outlined in Appendix A. [10] Here the computations are more complicated since there is now one-loop mixing between $\tilde{t}_1$ and $\tilde{t}_2$. In the EFT approach, one must decouple separately the two stops, and include the most general stop-mixing effects in the determination of the relation between the on-shell and $\overline{\rm MS}$ parameters. The leading $\mathcal{O}(m_t^2 h_t^4)$ corrections in the EFT approach can be incorporated as in Section 2 [14,15] by extending the computations of Appendix A to include the one-loop $\mathcal{O}(h_t^2)$ corrections to the running top-quark mass and stop sector parameters. However, at present, one cannot

[10] The transformation from on-shell to $\overline{\rm MS}$ input parameters for the case of the most general stop squared-mass matrix will be included in the new version of the program *FeynHiggs*.

check these results against an $\mathcal{O}(m_t^2 h_t^4)$ two-loop diagrammatic computation, since the latter does not yet appear in the literature in full generality.

Going beyond the approximations made in this paper, the next step is to incorporate the above improvements, as well as the next subleading contributions of $\mathcal{O}(m_Z^2 h_t^2 \alpha_s)$ and $\mathcal{O}(m_Z^2 h_t^4)$ into the computation of $m_h^2$. One might then hope to show that a complete mixed-scale one-loop EFT result, suitably generalized, provides a very good approximation to the radiatively-corrected $\mathcal{CP}$-even Higgs mass of the MSSM. Such an analysis could be used to organize the most significant non-leading one-loop and two-loop contributions to $m_h^2$ and provide some insight regarding the magnitude of the unknown higher-order corrections, thus reducing the theoretical uncertainty in the prediction for $m_h$. This would have a significant impact on the physics of the lightest $\mathcal{CP}$-even Higgs boson at LEP2, the upgraded Tevatron and the LHC.

## Note added

After this work was completed, we received a paper [38] which discusses many of the same issues that we address in this work. In Ref. [38], the two-loop effective potential of the MSSM is employed, including renormalization group resummation of logarithmic terms, and the leading nonlogarithmic two-loop terms of $\mathcal{O}(\alpha\alpha_s)$. The relation between on-shell and $\overline{\rm MS}$ parameters are also taken into account. The end results are qualitatively similar to the ones obtained here.

## Acknowledgements

M.C., H.E.H. and C.W. would like to thank the Aspen Center for Physics, where part of this work has been carried out. The work of M.C., H.E.H. and C.W. is supported in part by the US Department of Energy. W.H. gratefully acknowledges support by the Volkswagenstiftung. H.E.H. and S.H. thankfully acknowledge hospitality of the CERN Theory Group, where a major part of this work was completed. H.E.H. is pleased to acknowledge useful discussions with Damien Pierce.

## Appendix A. Relations between on-shell and $\overline{\rm MS}$ definitions of $m$, $M_S$ and $X_t$

In this appendix, we derive the relations between the on-shell and $\overline{\rm MS}$ definitions of $m_t$, $M_S$ and $X_t$. We have checked that these results agree with similar results given in Ref. [9]. These results are derived in a model where the stop mass-squared matrix is given by Eq. (6). The corresponding stop squared-masses and mixing angle are given by Eqs. (7) and (8). Note that in this model, the top-squark mass eigenstates, $\tilde{t}_1$ and $\tilde{t}_2$, are states of definite parity in their interactions with gluons and gluinos. The corresponding Feynman rules are shown in Fig. 3.

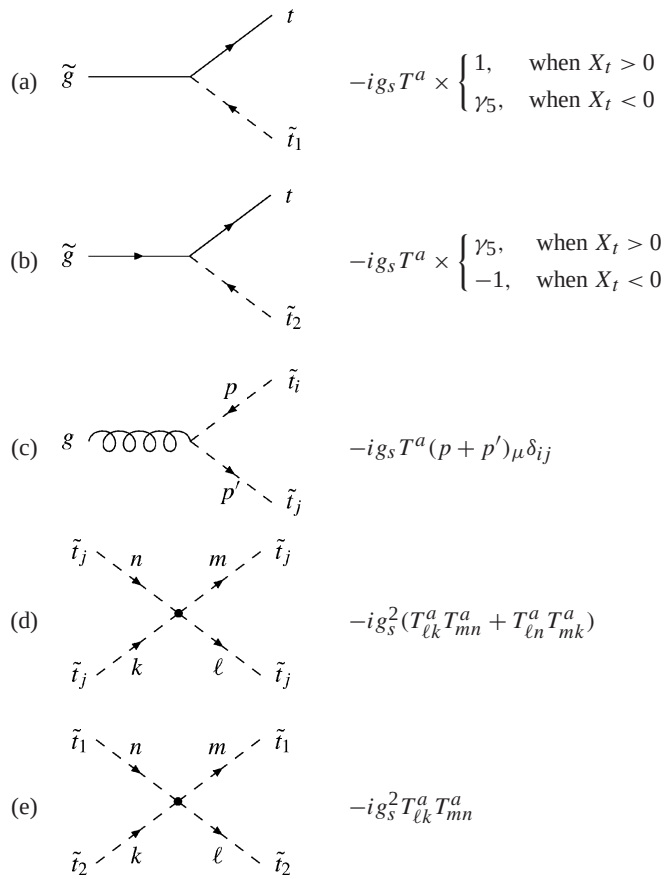


Fig. 3. Feynman rules for top-squark interactions in a model where the stop mass-squared matrix is given by Eq. (6).

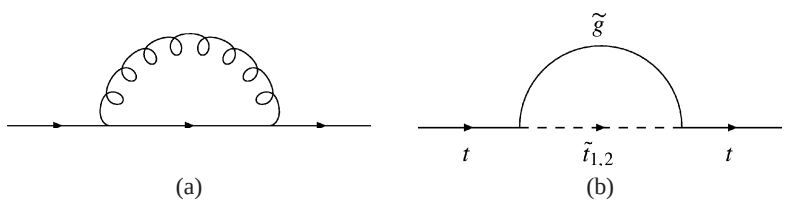


Fig. 4. One-loop contributions to the top quark mass.

Consider first the one-loop contribution to the top-quark two-point function at $\mathcal{O}(\alpha_s)$ due to: (i) the top-quark/gluon loop (Fig. 4(a)) and (ii) the stop/gluino loop (Fig. 4(b)). Divergences are regulated by dimensional regularization in $D \equiv 4 - 2\varepsilon$ dimensions and removed by minimal subtraction. Including the tree-level contribution (which is equal to the negative of the inverse tree-level propagator), the end result is: [11]

[11] All results in this section are given in the $\overline{\text{MS}}$ subtraction scheme. In the $\overline{\text{DR}}$ scheme, all the formulae of this

$$\begin{aligned}\Gamma^{(2)}(p) = i\big[\not{p} - \overline{m}_t(\mu)\big] \\ - \frac{iC_F\alpha_s}{4\pi}\Big\{\not{p}\big[1 + 2\mathcal{B}_1\big(p^2; m_t^2, 0\big)\big] - 2m_t\big[1 - 2\mathcal{B}_0\big(p^2; m_t^2, 0\big)\big] \\ + \not{p}\big[\mathcal{B}_1\big(p^2; m_{\tilde{g}}^2, M_S^2 - m_t X_t\big) + \mathcal{B}_1\big(p^2; m_{\tilde{g}}^2, M_S^2 + m_t X_t\big)\big] \\ - m_{\tilde{g}}\big[\mathcal{B}_1\big(p^2; m_{\tilde{g}}^2, M_S^2 - m_t X_t\big) - \mathcal{B}_1\big(p^2; m_{\tilde{g}}^2, M_S^2 + m_t X_t\big)\big]\Big\}, \qquad \text{(A.1)}\end{aligned}$$

where $T^a T^a = C_F \mathbf{1}$ is the $SU(3)$ quadratic Casimir operator in the fundamental representation, $C_F = 4/3$, and

$$\mathcal{B}_n\big(p^2; m_1^2, m_2^2\big) \equiv (-1)^{n+1} \int_0^1 dy\, y^n \ln\left(\frac{m_2^2 y + m_1^2(1-y) - p^2 y(1-y)}{\mu^2}\right). \qquad \text{(A.2)}$$

The $\mathcal{B}_n$ ($n = 0, 1$) are related to the standard two-point loop functions that arise in one-loop computations (our conventions for the loop functions follow those of [39]):

$$\begin{aligned} B_0\big(p^2; m_1^2, m_2^2\big) &\equiv \Delta + \mathcal{B}_0\big(p^2; m_1^2, m_2^2\big), \\ B_1\big(p^2; m_1^2, m_2^2\big) &\equiv -\tfrac{1}{2}\Delta + \mathcal{B}_1\big(p^2; m_1^2, m_2^2\big), \end{aligned} \qquad \text{(A.3)}$$

where all occurrences of $\Delta \equiv (4\pi)^{\varepsilon}\Gamma(\varepsilon)$ are removed in the minimal subtraction procedure. Note that $B_0(p^2; m_1^2, m_2^2)$ is invariant under the interchange of $m_1^2$ and $m_2^2$, whereas

$$B_1\big(p^2; m_2^2, m_1^2\big) = -B_1\big(p^2; m_1^2, m_2^2\big) - B_0\big(p^2; m_1^2, m_2^2\big). \qquad \text{(A.4)}$$

In Eq. (A.1), $\mu$ is the arbitrary mass parameter of the $\overline{\text{MS}}$-scheme. The on-shell top-quark mass, $M_t$, is defined by $\Gamma^{(2)}(\not{p} = M_t) = 0$. It follows that

$$\begin{aligned} M_t = \overline{m}_t(\mu) + \frac{C_F\alpha_s m_t}{4\pi}\Big\{4\mathcal{B}_0\big(m_t^2; m_t^2, 0\big) + 2\mathcal{B}_1\big(m_t^2; m_t^2, 0\big) - 1 \\ + \mathcal{B}_1\big(m_t^2; m_{\tilde{g}}^2, M_S^2 - m_t X_t\big) + \mathcal{B}_1\big(m_t^2; m_{\tilde{g}}^2, M_S^2 + m_t X_t\big) \\ - \frac{m_{\tilde{g}}}{m_t}\big[\mathcal{B}_0\big(m_t^2; m_{\tilde{g}}^2, M_S^2 - m_t X_t\big) - \mathcal{B}_0\big(m_t^2; m_{\tilde{g}}^2, M_S^2 + m_t X_t\big)\big]\Big\}. \qquad \text{(A.5)}\end{aligned}$$

In the $\mathcal{O}(\alpha_s)$ terms above, we simply use the generic notation $m_t$ for the top-quark mass, since to one-loop accuracy one need not distinguish between $\alpha_s M_t$ and $\alpha_s m_t(\mu)$. As previously noted, the relation between the top-quark mass in the on-shell and $\overline{\text{DR}}$ schemes is obtained by dropping the $-1$ (which does not multiply a loop-function) in Eq. (A.5).

Two of the loop functions are easily evaluated: $\mathcal{B}_0(m_t^2; m_t^2, 0) = 2 - \ln(m_t^2/\mu^2)$ and $\mathcal{B}_1(m_t^2; m_t^2, 0) = -\frac{1}{2}[3 - \ln(m_t^2/\mu^2)]$. We note the following curious fact. In the supersymmetric limit ($m_{\tilde{t}_1} = m_{\tilde{t}_2} = m_t$ and $m_{\tilde{g}} = 0$) at one-loop, the relation between the on-shell and $\overline{\text{DR}}$ running top-quark mass evaluated at $\mu = m_t$ is precisely the same as the corresponding relation between the on-shell and $\overline{\text{MS}}$ running top-quark mass in non-supersymmetric QCD.

appendix still apply except in the case of the top-quark gluon loop. To obtain the corresponding $\overline{\text{DR}}$ result, simply remove the additive factors of 1 in the two occurrences in Eq. (A.1).

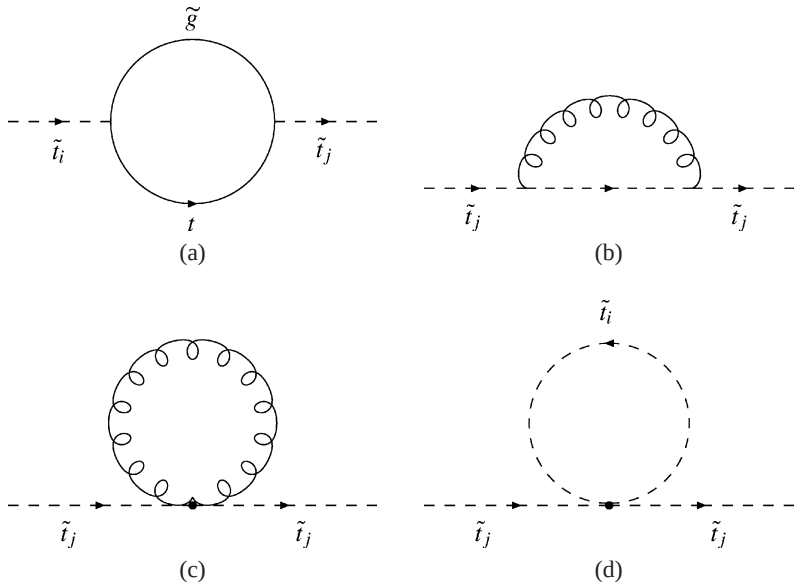


Fig. 5. One-loop contributions to the top squark mass.

Next, we examine the one-loop contributions to the top-squark two-point function at $\mathcal{O}(\alpha_s)$. The contributing graphs are shown in Fig. 5. We immediately note that graph (c) of Fig. 5 vanishes in dimensional regularization. Moreover, since $\tilde{t}_1$ and $\tilde{t}_2$ are states of definite parity in a model where the stop mass-squared matrix is given by Eq. (6), the one-loop mixing of $\tilde{t}_1$ and $\tilde{t}_2$ vanishes to all orders in $\alpha_s$. Including the tree-level contribution, the final result for the top squark two-point function is [12]

$$\begin{aligned}\widetilde{\Gamma}^{(2)}_{jj}(p^2) = i\big(p^2 - m^2_{\tilde{t}_j}\big) &\\ - \frac{iC_F\alpha_s}{\pi}\Big[&\mathcal{A}_0\big(m^2_{\tilde{g}}\big) + m_t^2\mathcal{B}_0\big(p^2; m_t^2, m^2_{\tilde{g}}\big) + p^2\mathcal{B}_1\big(p^2; m_t^2, m^2_{\tilde{g}}\big)\\ &- (-1)^j m_{\tilde{g}} m_t \mathcal{B}_0\big(p^2; m_t^2, m^2_{\tilde{g}}\big) - p^2\mathcal{B}_1\big(p^2; m^2_{\tilde{t}_j}, 0\big)\Big],\end{aligned} \tag{A.6}$$

for $j = 1, 2$, where

$$\mathcal{A}_0\big(m^2\big) \equiv m^2\left[1 - \ln\left(\frac{m^2}{\mu^2}\right)\right] \tag{A.7}$$

is related to the standard one-point loop function $A_0(m^2) = m^2\Delta + \mathcal{A}_0(m^2)$.

There is no distinction in this calculation between the $\overline{\rm MS}$ and $\overline{\rm DR}$ schemes. The on-shell stop squared-masses are defined by $\widetilde{\Gamma}^{(2)}_{jj}(p^2 = (m^{\rm OS}_{\tilde{t}_j})^2) = 0$. Noting the form for the tree-level squared-masses (Eq. (7)), it follows that

[12] In deriving Eq. (A.6), we note that the contribution of Fig. 5(d) (only the case $i = j$ yields a nonzero contribution, which is equal to $(iC_F\alpha_s/4\pi)\mathcal{A}_0(m_{\tilde{t}_j})$) cancels a similar term that arises in the evaluation of Fig. 5(b).

$$M_S^{2,\mathrm{OS}} \mp M_t X_t^{\mathrm{OS}} = \overline{M}_S^2(\mu) \mp \overline{m}_t(\mu)\overline{X}_t(\mu) + \frac{C_F\alpha_s}{\pi}\big[f\big(M_S^2 \mp m_t X_t\big) \pm g\big(M_S^2 \mp m_t X_t\big)\big], \tag{A.8}$$

where $M_t$ is the on-shell top quark mass and

$$f\big(p^2\big) \equiv \mathcal{A}_0\big(m_{\tilde{g}}^2\big) + m_t^2\mathcal{B}_0\big(p^2; m_t^2, m_{\tilde{g}}^2\big) + p^2\mathcal{B}_1\big(p^2; m_t^2, m_{\tilde{g}}^2\big),$$
$$g\big(p^2\big) \equiv m_{\tilde{g}} m_t \mathcal{B}_0\big(p^2; m_t^2, m_{\tilde{g}}^2\big). \tag{A.9}$$

It is then straightforward to solve for $M_S^{2,\mathrm{OS}}$ and $M_t X_t^{\mathrm{OS}}$ in terms of the corresponding $\overline{\mathrm{MS}}$ quantities evaluated at the scale $\mu = M_S$. Using the notation of Eq. (25), we obtain:

$$M_S^{2,\mathrm{OS}} = \overline{M}_S^2 + \frac{C_F\alpha_s}{2\pi}\big[f\big(M_S^2 + m_t X_t\big) + f\big(M_S^2 - m_t X_t\big) - g\big(M_S^2 + m_t X_t\big) + g\big(M_S^2 - m_t X_t\big)\big], \tag{A.10}$$

$$M_t X_t^{\mathrm{OS}} = \overline{m}_t(M_S)\overline{X}_t + \frac{C_F\alpha_s}{2\pi}\big[f\big(M_S^2 + m_t X_t\big) - f\big(M_S^2 - m_t X_t\big). - g\big(M_S^2 + m_t X_t\big) - g\big(M_S^2 - m_t X_t\big)\big], \tag{A.11}$$

where all loop functions in Eqs. (A.10) and (A.11) are evaluated at $\mu = M_S$. Dividing Eq. (A.11) by $M_t$, and using Eq. (A.5) to evaluate $\overline{m}_t(M_S)/M_t$, one obtains a direct relation between $X_t^{\mathrm{OS}}$ and $\overline{X}_t$.

To obtain the expansions derived in Appendix B, we consider the case of $m_{\tilde{g}}^2 = M_{\mathrm{SUSY}}^2 = M_S^2 - m_t^2$. We introduce the following notation:

$$x_t \equiv \frac{X_t}{M_S}, \qquad z \equiv \frac{M_t}{M_S}. \tag{A.12}$$

We are interested in the limit of $z \ll 1$ and $x_t \lesssim 1$. First, consider the relation between the on-shell and running top quark mass. Using Eq. (A.2), we must evaluate the following integrals:

$$J_n^{(\pm)} = \int_0^1 dy\, y^n \ln\big[1 \pm x_t z y - z^2\big(1 - y^2\big)\big], \tag{A.13}$$

for $n = 0, 1$. Eq. (A.5) then yields:

$$\overline{m}_t(M_S) = M_t\left\{1 + \frac{C_F\alpha_s}{4\pi}\left[-4 + 6\ln z - J_1^{(+)} - J_1^{(-)} + \frac{1}{z}\big(1 - z^2\big)^{1/2}\big(J_0^{(+)} - J_0^{(-)}\big)\right]\right\}. \tag{A.14}$$

Expanding out the logarithm in the integrand of $J_n^{(\pm)}$ in a double power series in $x_t$ and $z$ and integrating term by term, one readily obtains the result given in Eq. (B.5).

Second, consider the relation between the on-shell and $\overline{\mathrm{MS}}$ definitions of $M_S$ and $X_t$ obtained in Eq. (A.10). Using the integral expressions for the loop functions that appear in Eq. (A.9), one must evaluate the following integrals:

$$I_n = \int_0^1 dy\, y^n \ln\bigl[y^2(1-zx_t) + yz(x_t-2z) + z^2\bigr], \tag{A.15}$$

for $n = 0$, 1. In this case, one cannot simply expand the logarithms about $x_t = z = 0$, since the integration range extends down to $y = 0$. Instead, we have used *Mathematica* to evaluate the integral exactly, and then perform the double expansion in $x_t$ and $z$. The result for $I_0$ up to $\mathcal{O}(x_t^2 z^4)$ is

$$\begin{aligned} I_0 = {} & -2 + \pi z + z^2(2\ln z - 1) - \tfrac{1}{2}\pi z^3 + \tfrac{1}{2}z^4 \\ & + x_t\bigl[-z - z\ln z + \pi z^2 + z^3\bigl(2\ln z - \tfrac{1}{2}\bigr) - \tfrac{1}{2}\pi z^4\bigr] \\ & + x_t^2\bigl[-\tfrac{1}{8}\pi z - z^2(\ln z + 1) + \tfrac{15}{16}\pi z^3 + z^4\bigl(2\ln z - \tfrac{1}{2}\bigr)\bigr] \\ & + x_t^3\bigl[\tfrac{1}{12}z - \tfrac{1}{8}\pi z^2 - z^3\bigl(\ln z + \tfrac{11}{12}\bigr) + \tfrac{15}{16}\pi z^4\bigr] \\ & + x_t^4\bigl[-\tfrac{1}{128}\pi z + \tfrac{1}{12}z^2 - \tfrac{35}{256}\pi z^3 - z^4\bigl(\ln z + \tfrac{11}{12}\bigr)\bigr]. \end{aligned} \tag{A.16}$$

We have checked the validity of this expansion using numerical integration. One can derive a similar expression for $I_1$ either directly, or by noting that:

$$\begin{aligned} I_1 = {} & \frac{1}{2(1-zx_t)}\bigl[z^2(1-2\ln z) - \bigl(1-z^2\bigr)\bigl[1 - \ln\bigl(1-z^2\bigr)\bigr] - z(x_t - 2z)I_0\bigr] \\ = {} & -\tfrac{1}{2} - z^2\bigl(\ln z + \tfrac{3}{2}\bigr) + \pi z^3 + z^4\bigl(2\ln z - \tfrac{3}{4}\bigr) \\ & + x_t\bigl[\tfrac{1}{2}z - \tfrac{1}{2}\pi z^2 - z^3(3\ln z + 2) + \tfrac{9}{4}\pi z^4\bigr] \\ & + x_t^2\bigl[\tfrac{1}{2}z^2(\ln z + 2) - \tfrac{9}{8}\pi z^3 - z^4\bigl(5\ln z + \tfrac{11}{4}\bigr)\bigr] \\ & + x_t^3\bigl[\tfrac{1}{16}\pi z^2 + z^3\bigl(\ln z + \tfrac{19}{12}\bigr) - \tfrac{55}{32}\pi z^4\bigr] \\ & + x_t^4\bigl[-\tfrac{1}{24}z^2 + \tfrac{15}{128}\pi z^3 + z^4\bigl(\tfrac{3}{2}\ln z + \tfrac{17}{8}\bigr)\bigr]. \end{aligned} \tag{A.17}$$

Inserting these results into Eqs. (A.10) and (A.11), and expanding out the remaining factors (e.g., $m_{\tilde{g}} m_t = M_S^2 z(1-z^2)^{1/2}$, etc.), one ends up with the results given in Eqs. (B.3) and (B.4).

## Appendix B. Results up to $\mathcal{O}\bigl(m_t^4/M_S^4\bigr)$

We list the necessary formulae in order to derive the results given in Sections 3 and 4 up to terms of $\mathcal{O}(m_t^4/M_S^4)$. As before, we define $x_t \equiv X_t/M_S$ and $z \equiv m_t/M_S$. In the approximation discussed in Section 3, we obtain expansions that are valid in the limit of $z \ll 1$ and $x_t \lesssim 1$.

The diagrammatic result in the on-shell scheme for the one-loop and two-loop contributions to ${m_h}^2$, in the approximations used in this paper, is given up to $\mathcal{O}(z^4)$ by

$$m_h^{2,\alpha} = \frac{3}{2}\frac{G_F\sqrt{2}}{\pi^2} M_t^4 \bigl\{-2\ln z + x_t^2\bigl[1 - \tfrac{1}{12}x_t^2 - z^2\bigl(\tfrac{1}{2} - \tfrac{1}{3}x_t^2\bigr) - \tfrac{1}{4}z^4 x_t^2\bigr]\bigr\}, \tag{B.1}$$

$$
\begin{aligned}
m_h^{2,\alpha\alpha_s} = -3\frac{G_F\sqrt{2}}{\pi^2}\frac{\alpha_s}{\pi}M_t^4\big\{&4\ln^2 z \\
&+\big[-4-2x_t^2+\tfrac{1}{9}z^2\big(6+42x_t+33x_t^2-26x_t^3-18x_t^4\big) \\
&+\tfrac{1}{9}z^4\big(2-41x_t-10x_t^2+91x_t^3+45x_t^4\big)\big]\ln z \\
&-\tfrac{1}{4}x_t\big(8-x_t^3\big)+\tfrac{1}{36}\pi z x_t\big(48+24x_t-14x_t^2-7x_t^3\big) \\
&+\tfrac{1}{36}z^2x_t\big(60-6x_t-106x_t^2-61x_t^3\big) \\
&-\tfrac{1}{72}\pi z^3x_t\big(192+72x_t-236x_t^2-111x_t^3\big) \\
&+\tfrac{1}{36}z^4x_t\big(57+34x_t+95x_t^2+20x_t^3\big)\big\}. \qquad \text{(B.2)}
\end{aligned}
$$

Eq. (B.2) is a generalization of the corresponding formula given in Ref. [20].

The relations between the $\overline{\rm MS}$ parameters $\overline{M}_S$ and $\overline{X}_t$ (Eq. (25)) and the corresponding on-shell parameters $M_S^{\rm OS}$, $X_t^{\rm OS}$ can be obtained from Eqs. (A.10) and (A.11) using the expansions of Eqs. (A.16) and (A.17). The end result up to $\mathcal{O}(z^4)$ is given by

$$
\begin{aligned}
\overline{M}_S^2 = M_S^{2,\rm OS}\bigg\{1+\frac{2\alpha_s}{3\pi}\big[&-4-\tfrac{1}{12}z^2\big(12+24x_t+6x_t^2-2x_t^3-x_t^4\big) \\
&+\tfrac{1}{8}\pi z^3x_t\big(16+8x_t-2x_t^2-x_t^3\big)+\tfrac{1}{12}z^4\big(6-6x_t^2-23x_t^3-10x_t^4\big) \\
&+\big[z^2\big(2-2x_t-x_t^2\big)+z^4x_t\big(5+2x_t-2x_t^2-x_t^3\big)\big]\ln z\big]\bigg\}, \qquad \text{(B.3)}
\end{aligned}
$$

$$
\begin{aligned}
\overline{X}_t = X_t^{\rm OS}&\frac{m_t^{\rm OS}}{m_t^{\overline{\rm MS}}(M_S)} \\
&+\frac{2\alpha_s}{3\pi}M_S\big\{4-\tfrac{1}{64}\pi z\big(128+64x_t-16x_t^2-8x_t^3-x_t^4\big) \\
&\quad+\tfrac{1}{6}z^2x_t\big(6+12x_t+4x_t^2-x_t^3\big) \\
&\quad+\tfrac{1}{64}\pi z^3\big(128+32x_t-128x_t^2-60x_t^3+17x_t^4\big) \\
&\quad-\tfrac{1}{12}z^4\big(30+6x_t-6x_t^3-23x_t^4\big) \\
&\quad+\big[z^2(2+x_t)\big(-2+x_t^2\big)+z^4\big(2-5x_t^2-2x_t^3+2x_t^4\big)\big]\ln z\big\}. \qquad \text{(B.4)}
\end{aligned}
$$

To complete the evaluation of $\overline{X}_t$ we need to find a relation between the on-shell top-quark mass, $M_t$, and the running top-quark mass, $\overline{m}_t(M_S)$, evaluated at the scale $M_S$. Using Eq. (A.14), one obtains the following expansion:

$$
\begin{aligned}
\overline{m}_t(M_S) = M_t\bigg\{1+\frac{\alpha_s}{3\pi}\big[&-4+6\ln z+x_t+z^2\big(\tfrac{1}{2}+\tfrac{1}{4}x_t^2+\tfrac{1}{6}x_t^3\big) \\
&+z^4\big(\tfrac{1}{6}-\tfrac{1}{24}x_t+\tfrac{1}{6}x_t^2+\tfrac{1}{12}x_t^3+\tfrac{1}{12}x_t^4+\tfrac{1}{15}x_t^5\big)\big]\bigg\}. \qquad \text{(B.5)}
\end{aligned}
$$

Eq. (B.5) was derived using DREG. In order to obtain the corresponding formula using DRED (which yields a formula for the top-quark mass in the $\overline{\rm DR}$ scheme), simply replace $-4$ with $-5$ in the first term of Eq. (B.5) after the left square bracket.

Note that Eq. (B.5) provides a connection between $\overline{m}_t(M_S)$ and the on-shell mass $M_t$ in the full supersymmetric theory. In the limit of large $M_S$ with fixed $X_t/M_S$, the threshold

correction arising from the stop mixing effects does not vanish. On the other hand, the $\overline{\rm MS}$ top-quark mass, $\overline{m}_t \equiv m^{\overline{\rm MS}}_{t,{\rm SM}}(M_t)$ is defined in the low-energy (non-supersymmetric) effective theory via Eq. (3). Thus, in Eq. (B.5), we may replace $M_t$ with $\overline{m}_t$ simply by removing the factor of $-4\alpha_s/3\pi$. To leading order in $m_t/M_S$, one immediately obtains Eq. (43).

## References


[1] P. McNamara [speaking for the LEP Higgs Working Group], LEP Higgs Working Group Status Report, presentation at the LEPC meeting at CERN, 7 September 1999.
[2] A. Blondel, ALEPH in 1999, presentation at the LEPC meeting at CERN, 9 November 1999, http://alephwww.cern.ch/~bdl/lepc/lepc.ppt.
[3] H.E. Haber, R. Hempfling, Phys. Rev. Lett. 66 (1991) 1815.
[4] Y. Okada, M. Yamaguchi, T. Yanagida, Prog. Theor. Phys. 85 (1991) 1.
[5] J. Ellis, G. Ridolfi, F. Zwirner, Phys. Lett. B 257 (1991) 83, Phys. Lett. B 262 (1991) 477.
[6] R. Barbieri, M. Frigeni, Phys. Lett. B 258 (1991) 395.
[7] P. Chankowski, S. Pokorski, J. Rosiek, Nucl. Phys. B 423 (1994) 437.
[8] A. Dabelstein, Nucl. Phys. B 456 (1995) 25, Z. Phys. C 67 (1995) 495.
[9] J. Bagger, K. Matchev, D. Pierce, R. Zhang, Nucl. Phys. B 491 (1997) 3.
[10] M. Quirós, in: G.L. Kane (Ed.), Perspectives on Higgs Physics II, World Scientific, Singapore, 1997, pp. 148–180.
[11] H.E. Haber, R. Hempfling, Phys. Rev. D 48 (1993) 4280.
[12] J. Casas, J. Espinosa, M. Quirós, A. Riotto, Nucl. Phys. B 436 (1995) 3, Eratum: Nucl. Phys. B 439 (1995) 466.
[13] M. Carena, J. Espinosa, M. Quirós, C. Wagner, Phys. Lett. B 355 (1995) 209.
[14] M. Carena, M. Quirós, C. Wagner, Nucl. Phys. B 461 (1996) 407.
[15] H.E. Haber, R. Hempfling, A. Hoang, Z. Phys. C 75 (1997) 539.
[16] R. Hempfling, A. Hoang, Phys. Lett. B 331 (1994) 99.
[17] S. Heinemeyer, W. Hollik, G. Weiglein, Phys. Rev. D 58 (1998) 091701.
[18] S. Heinemeyer, W. Hollik, G. Weiglein, Phys. Lett. B 440 (1998) 296.
[19] S. Heinemeyer, W. Hollik, G. Weiglein, Eur. Phys. J. C 9 (1999) 343.
[20] S. Heinemeyer, W. Hollik, G. Weiglein, Phys. Lett. B 455 (1999) 179.
[21] R.-J. Zhang, Phys. Lett. B 447 (1999) 89.
[22] C. Bollini, J. Giambiagi, Nuovo Cimento B 12 (1972) 20.
[23] J. Ashmore, Nuovo Cimento Lett. 4 (1972) 289.
[24] G. 't Hooft, M. Veltman, Nucl. Phys. B 44 (1972) 189.
[25] B. Schrempp, M. Wimmer, Prog. Part. Nucl. Phys. 37 (1996) 1.
[26] W. Siegel, Phys. Lett. B 84 (1979) 193.
[27] D. Capper, D.R.T. Jones, P. van Nieuwenhuizen, Nucl. Phys. B 167 (1980) 479.
[28] H.E. Haber, in: J. Solà (Ed.), Proc. Fourth Int. Symp. Radiative Corrections: Application of Quantum Field Theory to Phenomenology, RADCOR 98, Universitat Autónoma de Barcelona, Barcelona, Catalonia, Spain, 8–12 September 1998, World Scientific, Singapore, 1999, pp. 425–440.
[29] S. Heinemeyer, W. Hollik, G. Weiglein, Comput. Phys. Commun. 124 (2000) 76.
[30] S. Heinemeyer, W. Hollik, G. Weiglein, DESY 99-120, hep-ph/9909540.
[31] M. Carena, S. Mrenna, C.E.M. Wagner, Phys. Rev. D 60 (1999) 075010.
[32] M. Carena, S. Mrenna, C.E.M. Wagner, hep-ph/9907422.
[33] K.S. Babu, C. Kolda, Phys. Lett. B 451 (1999) 77.
[34] F. Borzumati, G.R. Farrar, N. Polonsky, S. Thomas, Nucl. Phys. B 555 (1999) 53.

[35] H. Eberl, K. Hidaka, S. Kraml, W. Majerotto, Y. Yamada, HEPHY-PUB-725-99, hep-ph/9912463.
[36] M. Carena, D. Garcia, U. Nierste, C.E.M. Wagner, FERMILAB-PUB-99-367-T, hep-ph/9912516.
[37] A. Pilaftsis, C.E.M. Wagner, Nucl. Phys. B 553 (1999) 3.
[38] J.R. Espinosa, R.-J. Zhang, JHEP 0003 (2000) 026.
[39] W. Hollik, in: P. Langacker (Ed.), Precision Tests of the Standard Electroweak Model, World Scientific, Singapore, 1995, pp. 37–116.